ISSN 0869-5911, Petrology, 2006, Vol. 14, No. 6, pp. 540–566. © Pleiades Publishing, Inc., 2006.
Original Russian Text © V.I. Fel'dman, L.V. Sazonova, E.A. Kozlov, 2006, published in Petrologiya, 2006, Vol. 14, No. 6, pp. 576–603.

Shock Metamorphism of Some Rock-Forming Minerals: Experimental Results and Natural Observations

V. I. Fel'dman[a], L. V. Sazonova[a], and E. A. Kozlov[b]

[a] *Faculty of Geology, Moscow State University, Vorob'evy gory, Moscow, 119899 Russia*

e-mail: saz@geol.msu.ru, feldman@geol.msu.ru

[b] *Russian Federal Center for Nuclear Research—Zababakhin Institute of Technical Physics, Snezhinsk, Chelyabinsk oblast, 456770 Russia*

e-mail: kozlov@gdd.ch70.chel.ru

Received June 16, 2005

Abstract—The products of shock metamorphism in the Jänisjärvi astrobleme in Karelia, Russia, are compared with the results of experiments in which spherical converging shock waves affected a spherical rock sample. The sample was loaded by a broad spectrum of shock pressures, which increased from ~20 GPa at the periphery of the rock sphere to >200 GPa at its center. Experiments with rocks metamorphosed under the effect of spherical converging shock waves imitate collisions of cosmic bodies with the Earth's surface, when transformations in rocks and minerals are induced by a single impact event. The shock–thermal decomposition of mafic minerals occurs in the same succession in nature and the experiments, with some differences between natural and experimentally produced shock–thermal aggregates likely accounted for by the smaller sizes of the experimental impact rock sample and, correspondingly, its more rapid quenching. Our shock experiments were the first to synthesize ringwoodite that was rich in Al_2O_3 and should be referred to as aluminous ringwoodite. The mineral was produced not via the martensite transition of olivine but by means of biotite replacement coupled with the migration of elements. The transformations of minerals by shock waves (amorphization and shock–thermal decomposition) were determined to be controlled mainly by the crystal structures of these minerals. The experimental products provide evidence of the migration of chemical elements within the crystal structure. The structural setting of ions in a mineral determines the onset of element migrations and the intensity of this process.

DOI: 10.1134/S0869591106060038

INTRODUCTION

The parameters of shock metamorphism in naturally occurring impact structures (astroblemes) can be quantified using corresponding geothermometers and geobarometers, which can be calibrated only in laboratory experiments. However, the results of these experiments always leave uncertain as to how precisely the experimental conditions and the transformations of the rocks and minerals imitate those occurring in nature. To elucidate this problem, we conducted experiments on the shock-wave loading of rocks collected within the targets of previously examined natural astroblemes and outside them. The products of these shock experiments were then compared with shock-metamorphosed rocks and minerals from the Jänisjärvi astrobleme in Karelia, Russia.

The study of impactites from the Jänisjärvi astrobleme (Kozlov et al., 1998; Fel'dman et al., 1987, 1988; Fel'dman and Sazonova, 1988; Sazonova et al., 1988; Feldman, 1994; e.a.) indicates that shock waves induce not only mechanical transformations of the target rocks but also their chemical alterations and phase transitions in them. These processes were examined in the laboratory by loading rock samples with spherical converging shock waves (Kozlov, 1999).

Experiments with spherical shock waves have an advantage over experiments with plane shock waves, first of all, because a single experimental rock sample (which has the shape of a sphere) is affected by a wide range of shock pressures, which increase along the radius of the sphere toward its center from ~20 to >200 GPa. This enables the experimentalist to accurately enough correlate the transformations induced in the rock and its minerals at the shock wave front with the distance along the radius, i.e., with the shock pressure (Sazonova et al., 1998; Kozlov et al., 1997). Furthermore, experiments with spherical converging shock waves can fairly realistically imitate naturally occurring transformations of rocks and minerals during single impact events induced by the collisions of cosmic projectiles with the Earth's surface.

We utilized this technique to study the chemical and phase transformations induced by shock waves in the major minerals of plagioclase–biotite–quartz schist with garnet and staurolite porphyroblasts (referred to as *schist* hereafter), one of the most ubiquitous target rocks of the Jänisjärvi astrobleme. This publication pre-

sents our results obtained on the shock-induced migration of chemical elements that occupy different crystal-chemical sites in the structures of various rock-forming minerals (plagioclase, biotite, staurolite, and garnet). This paper describes the changes that occurred in these minerals in the solid state, i.e., before the onset of their melting. It was demonstrated that the characteristics of the crystal structures of minerals are of crucial significance during the amorphization and shock–thermal decomposition of these minerals with the development of shock–thermal aggregates of newly formed phases, including such a high-pressure mineral as ringwoodite. We were the first to detect ringwoodite, a spinel of olivine composition (γ-olivine), in the products of shock-wave metamorphism.

The latest and the most comprehensive review of the mineralogy of impactites (Deutsch et al., 1998) provides no information on any analogous studies conducted somewhere else around the world.[1]

EXPERIMENTAL CONDITIONS OF SHOCK-WAVE LOADING AND STUDY TECHNIQUES

The experiments were conducted with a sample of a target rock from the Jänisjärvi astrobleme. A sphere 48 mm in diameter prepared of this rock (which had a density of ρ_{00} = 2.8 g/cm^3) was welded in vacuum (10^{-5} mm Hg) into sealed jacket of 6-mm-thick stainless steel (12KH18N10T), which was then covered by a layer of plastic explosive (HMX/Plastic Binder-9/1, ρ_{ex} = 1,86 g/cm^3) 10 mm thick (h_{ex}). In order to simultaneously initiate a shock wave at several points at the surface of the sample at a radius (R_{ex}) of 40 mm, we utilized a spherical system for explosion initiation (Litvinov et al., 1991; Kozlov, 1999). The compression of the rock lasted approximately 2 μs. After the experiment, the sample was quenched with an initial rate of the temperature decrease equal to 10^8–10^9°C/s, which ensured, on the one hand, the preservation of all of the newly formed phases and, on the other, eliminated the possibility of annealing, low-temperature hydrothermal alterations, etc.

After its loading with a spherical shock wave, relaxation, and cooling, the rock sphere was cut by diamond-impregnated circular saw in the meridional plane, whose polished surface was then used to analyze the transformations in the rock-forming minerals of the schist along the sphere radius, with the shock pressure increasing from the sphere periphery to its center.

The composition of minerals affected by a converging spherical shock wave was analyzed at the Laboratory of High-Resolution Analytical Techniques of the Department of Petrology, Geological Faculty, Moscow State University, on a CamScan-4DV electron microscope equipped with a Link-AN 10000 EDS analytical system at an accelerating voltage of 15 kV and a beam current of (1–3) × 10^{-9} A. The analytical errors were ±2% at element concentrations of >10%, ±5% at concentrations from 5 to 10%, and ±10% at concentrations of 1–5%. Analyses were carried out at analytical spots with excitation areas ~3 μm in diameter and by means of scanning the sample over areas up to a few hundred square micrometers.

The Raman spectra of the ringwoodite were obtained on a LabRam spectrometer at the Bayerisches Geoinstitut in Bayreuth, Germany, using a 632-nm laser, 50× lens, and an 1.1-mm confocal slit. The examined region was approximately equal to 7 μm in the focal plane (to a depth of no less than 10 μm inward the sample) at a resolution of 2 cm^{-1} (Kozlov et al., 2002, 2003).

The raw analytical data were processed with mathematical statistical techniques. The concentrations of elements in minerals affected by different shock pressures were compared to elucidate the character of migration of these elements, with the use of only statistically significant values.

NATURAL OBSERVATIONS

Brief characterization of the Jänisjärvi astrobleme and its target rocks. The Jänisjärvi meteorite crater in Karelia (30 km north of Ladoga Lake) is now filled with the lake of Jänis (Jänisjärvi) approximately 13 × 17 km, which is slightly elongated to the southeast. Impactites are exposed at the central islands of the lake and the tip of the cape in its western part. The K–Ar isotopic age of the melt impactites is equal to 700 ± 5 Ma. The geology of this structure and the shock metamorphism of its target rocks were described in detail in (Fel'dman et al., 1987, 1988; Fel'dman and Sazonova, 1988; Sazonova et al., 1988; *Impactites*, 1981; *Geology…*, 1980; Fel'dman, 1990). Although this astrobleme shows no typical topographic features of a meteorite crater, it is clearly expressed in geophysical fields. Based on geophysical data, the initial diameter of this astrobleme was estimated at approximately 14 km (*Impactites*, 1981).

The target rocks of this astrobleme belong to the Pjalkjarvi and Naatselki formations of the Proterozoic Ladoga Group (1885 ± 30 Ma, Rb–Sr method). These formations (~1200 and 1000–1500 m thick, respectively) are composed of cyclically alternating mica–quartz schists. The rocks are commonly porphyroblastic and have a lepidogranoblastic matrix. The fine-grained (from a few tenths to a few hundredths of a millimeter) groundmass of the rocks usually consists of quartz and biotite, sometimes with muscovite and plagioclase and, very rarely, andalusite, sericite, and chlo-

[1] *And*—andalusite, *Bt*—biotite, *Crn*—corundum, *Cpx*—clinopyroxene, *Crd*—cordierite, *Cum*—cummingtonite, *Grs*—grossular, *Grt*—garnet, *Hc*—hercynite, *Ilm*—ilmenite, *Kfs*—potassic feldspar, *Opx*—orthopyroxene, *Pl*—plagioclase, *Qtz*—quartz, *Rw*—ringwoodite, *Spl*—spinel, *St*—staurolite, *STA*—shock–thermal aggregate(s).

rite. The porphyroblast minerals are garnet, staurolite, and biotite (Fig. 1a).

Quartz occurs as small (a few hundredths of a millimeter) anhedral grains in the rock matrix. *Biotite* is contained in the rock matrix and occurs as porphyroblasts, usually in the form of euhedral platelets up to 1.0×2.0 mm (in the groundmass) and 4.0×2.0 mm (in porphyroblasts). The mineral has pleochroism from pale yellow (N_p) to brown (N_g) and abounds in zircon inclusions surrounded by pleochroic halos. *Muscovite* is contained in some varieties of the schists but, in contrast to biotite, composes no porphyroblasts and is present only in the groundmass. The flakes of this mineral are no longer than 1.0 mm and are elongated parallel to the rock schistosity. *Plagioclase* composes small (no larger than 0.1–0.2 mm) anhedral grains in the rock matrix and contains 27–33% of the anorthite end member. *Staurolite* occurs as typical subhedral poikiloblasts of yellow color, up to 10×20 mm long (occasionally even longer). *Garnet* usually forms equant, sometimes euhedral porphyroblasts up to 1.0–2.0 mm across and is rare in the groundmass of the rock. The garnet is colorless in thin sections and pale pink to pinkish red in hand specimens. The accessory minerals in the rock matrix are magnetite, ilmenite, zircon, apatite, graphite, and tourmaline.

The mineral proportions of the schists notably vary: 35–55% quartz, 30–50% biotite, 3–12% muscovite, 0.5–9.0% garnet, and 0–15% plagioclase (*Impactites*, 1981).

The impactites are tagamites (remelted impactites), allogenic breccias, and suevites. Fragments in the suevites and breccias commonly range from 1.0 to 100 mm, sometimes being as large as a few decimeters or even meters. The fragments are mostly schists or, more rarely, quartzites, pegmatites, and recrystallized impact melt. Fragments of target rocks are angular or rounded and are not sorted and variably altered under the effect of shock pressures and postimpact temperatures. The cement of the suevite breccias consists of welded masses of fragments of the same rocks, quartz, and impact glass.

Diaplectic transformations of minerals in the fragments of the suevite breccias. The transformations examined in schist fragments from the suevites were induced in them by shock waves while the material of the fragments was still solid (so-called diaplectic transformations).

The leucocratic minerals (plagioclase and quartz) are characterized by such diaplectic alterations as fragmentation, planar deformations, and amorphization (origin of diaplectic glasses) (*Impactites*, 1981).

The mafic minerals (biotite, staurolite, and garnet) are characterized, in addition to fragmentation and planar deformations, also by their shock–thermal decomposition (Fel'dman and Sazonova, 1988; Fel'dman, 1990), i.e., the transformation of these minerals into extremely fine-grained (a few micrometers) aggregates of newly formed crystalline and amorphous phases. These aggregates completely inherit their morphologies from the pristine mineral grains (Fig. 1b).

Quartz. The quartz displays a clearly pronounced tendency toward a gradual decrease in its birefringence from 0.009 (in quartz from the unaltered target rocks) to 0.002 (in the shock-metamorphosed quartz). The refractive index n_e of the mineral decreases from 1.553 for the unaltered quartz to 1.546–1.547 for this mineral in samples most strongly affected by shock waves. The n_o refractive index ranges from 1.542 to 1.547 without any apparent tendencies or systematic variations. An increase in the shock pressures was determined to lead to an increase in the number of quartz grains of lower density (*Impactites*, 1981). As was mentioned above, diaplectic quartz displays numerous planar features along various crystallographic directions. The weighted mean shock pressure on a given rock sample was evaluated by the refractive index of quartz, with the use of the diagrams in (Stöffler, 1974), and by planar features and the appearance of quartz diaplectic glass. In the latter situation, the shock pressure was calculated by the formula

$$P_{\text{sh}}\,(\text{GPa}) = \frac{7.5A + 10.0B + 14.0C + 16.0D + 30.0E}{n},$$

where n is the overall number of measured quartz grains, A, B, C, and D are the numbers of quartz grains with planar features of variable orientation, and E is the number of quartz grains transformed into diaplectic glass. The formula proposed in (Grieve and Robertson, 1976) for the calculation of the weighted mean shock pressure on a rock with the use of quartz was corrected by introducing an additional term E. This drastically diminished the inaccuracies in the calculations of the pressures (Sazonova et al., 1982; Fel'dman et al., 1996).

The schist samples from the Jänisjärvi astrobleme that were examined in the course of this research contained biotite, staurolite, and garnet that were affected by average shock pressures in the range of 13–25 GPa (*Impactites*, 1981; Fel'dman et al., 1987, 1988). The after-shock temperature, which was evaluated based on its experimentally established dependence on shock pressure for quartz (*Impact Craters…*, 1983), was equal to 450–750°C.

Plagioclase. Diaplectic alterations in this mineral are expressed in the form of its amorphization and various mechanical deformations: fracturing, mechanical twinning, and planar features.

Biotite (Fig. 2). The transformations of biotite in suevite fragments from the Jänisjärvi astrobleme can be subdivided into two stages. During the *first stage*, the chemical composition of this mineral is modified but no newly formed phases appear. Biotite flakes were determined to acquire patches with lower K_2O concentrations, which are spatially restricted to mechanical deformations (kink bands and zones of intense fractur-

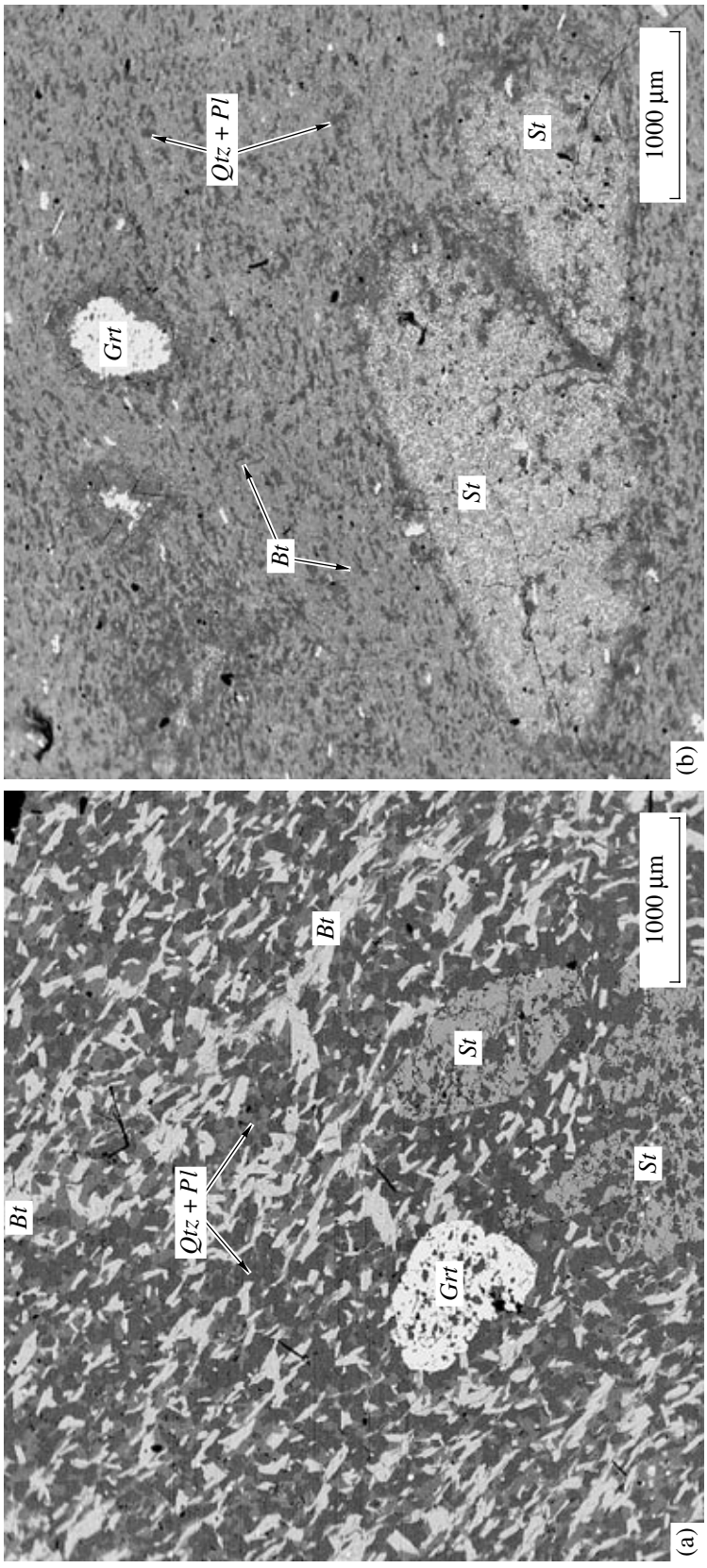

Fig. 1. Comparison of (a) unaltered and (b) impacted plagioclase–biotite–quartz schist with garnet and staurolite porphyroblasts from the Jänisjärvi astrobleme. In Fig. 1b, biotite, garnet, and staurolite are transformed into shock–thermal aggregates with variable intensities of pseudomorph alterations and look dissimilar to the minerals of the pristine schist.

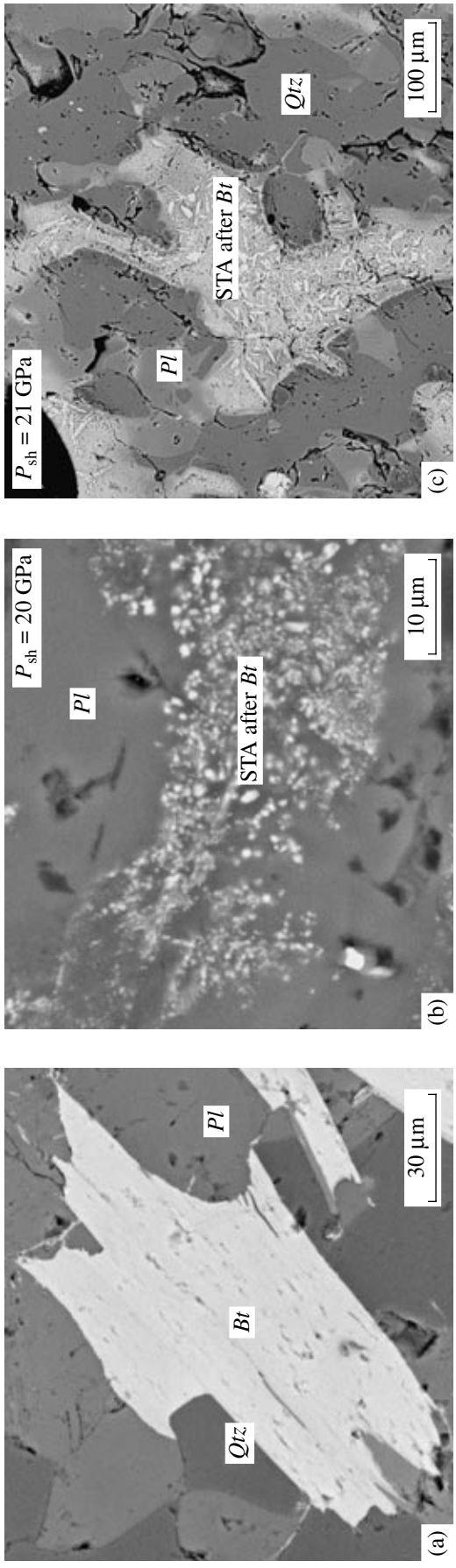

Fig. 2. Biotite from (a) the unaltered target schist, (b) shock–thermal aggregate (STA) replacing biotite in impacted schist from the Jänisjärvi astrobleme, and (c) schist affected by a shock wave in the experiment. In Fig. 2b, in STA replacing biotite from natural impacted schist, bright white is ilmenite, light gray is orthopyroxene, and darker gray is potassic feldspar. In Fig. 2c, in STA replacing biotite from experimental impacted schist, bright white elongated crystals are ringwoodite, and light gray is apobiotite residue.

ing) (Fel'dman et al., 1988). The transformations took place at shock pressures of 13–16 GPa. Moreover, Mössbauer spectroscopic data indicate that the biotite is characterized by a higher degree of iron oxidation (Granovsky et al., 1978), which is in good agreement with the increase in the degree of iron oxidation in the rock as a whole (Fel'dman et al., 1988).

During the *second stage*, biotite grains were modified more significantly and were transformed into aggregates of their decomposition products. Unaltered biotite relics remain among the decomposition products in the form of domains ranging from a few dozen to a few hundred micrometers across. The decomposition products of biotite were determined to include the following phases: ilmenite, sanidine, orthopyroxene, and a residue developing after biotite (apobiotite residues) (Fig. 3a). These transformations took place at shock pressures of 20 GPa and more. When this biotite is examined under an electron microscope, it can be seen that its decomposition begins along cracks. These can be either randomly oriented cracks or planar features that roughly or exactly follow certain crystallographic directions. The newly formed phases develop as chains along planar cracks. Sometimes they branch and define structures resembling reticulate ones. A single sample can contain variably altered biotite grains, from those with newly formed phases along single cracks to completely transformed grains. This definitely indicates that the pressure was unevenly distributed in the rock.

Staurolite (Figs. 4a–4c). The first alterations to occur in the staurolite are mechanical (extensive fracturing). As the shock pressures increased to 20–25 GPa, staurolite grains became turbid and acquired a brownish color, with light absorption in the visible region increasing to 80% (Fel'dman et al., 1978; Fel'dman, 1990). At even higher pressures, staurolite is gradually replaced by a mixture of sanidine, orthopyroxene, hercynite, and apobiotite residue (Fel'dman et al., 1978; Fel'dman, 1990) (Fig. 3b) with grains 1–5 μm in size.

Garnet (Fig. 5a, 5b). Garnet is the most resistant mineral in the shock metamorphosed target rocks of the Jänisjärvi astrobleme. At shock pressures of 13–25 GPa, garnet grains acquire extensive fracturing, including planar features (Fig. 5b). No chemical alterations of this mineral related to the passage of a shock wave were detected within this pressure range (Sazonova et al., 1988).

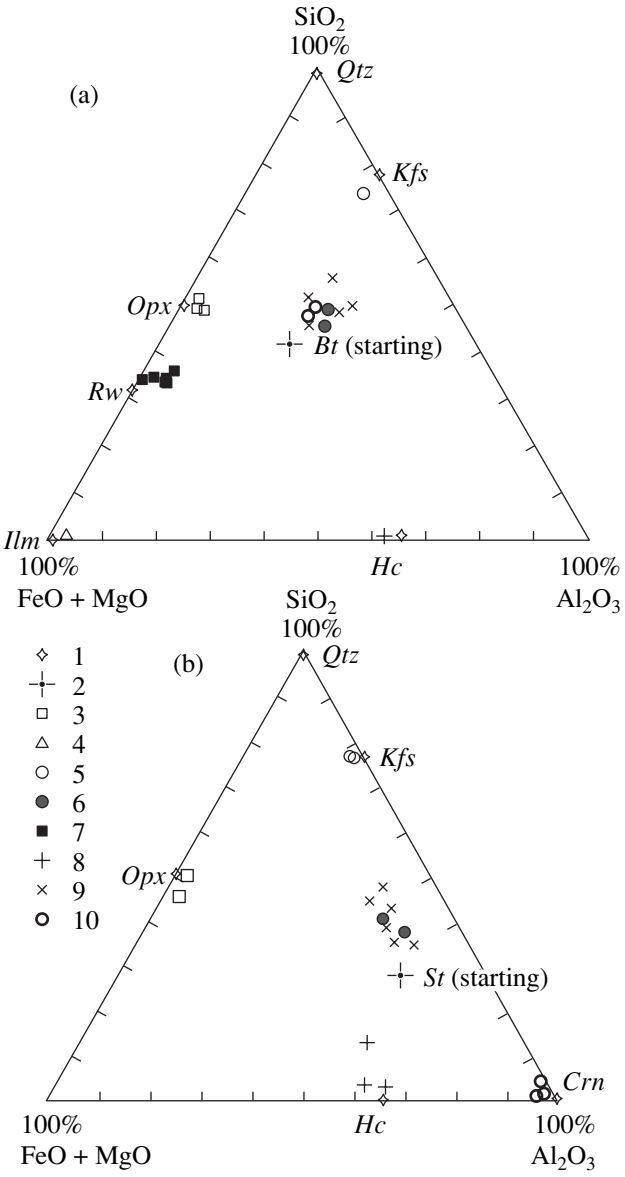

Fig. 3. Composition of shock–thermal aggregates of newly formed phases replacing (a) biotite and (b) staurolite in nature (suevite fragments from the Jänisjärvi astrobleme) and the experiment. (1) Theoretical composition of minerals; (2) composition of the original minerals. Jänisjärvi astrobleme: (3) *Opx*; (4) *Ilm*; (5) *Kfs*; (6) apobiotite and apostaurolite residue. Experiment: (7) *Rw*; (8) *Hc*; (9) apobiotite and apostaurolite residue; (10) *Crn*.

EXPERIMENTAL RESULTS

Shock-pressure adiabat of the rock. The rock sampled within the target of the Jänisjärvi astrobleme for the purposes of our experiments had a density (ρ_{00}) of 2.8 g/cm^3 and the following modal composition: 41.6% biotite, 35.9% quartz, 9.1% plagioclase, 6.3% staurolite, and 7.1% garnet. This composition corresponds to the average composition of the target schists of the astrobleme. Data on the density and chemical composition of the rock were used to calculate [using the method described in (Telegin et al., 1980)] the C_0 and λ coefficients in the equation for the state of the shock-compressed material (Hugoniot adiabat) $D = 2.584 + 1.596u$, where $C_0 = 2.584$ km/s, $\lambda = 1.596$, D is the shock wave velocity, and u is the velocity of material behind the shock wave front.

Variations in the shock pressure. The pressures and temperatures, which increased toward the center of the sphere along its radii, were calculated by the

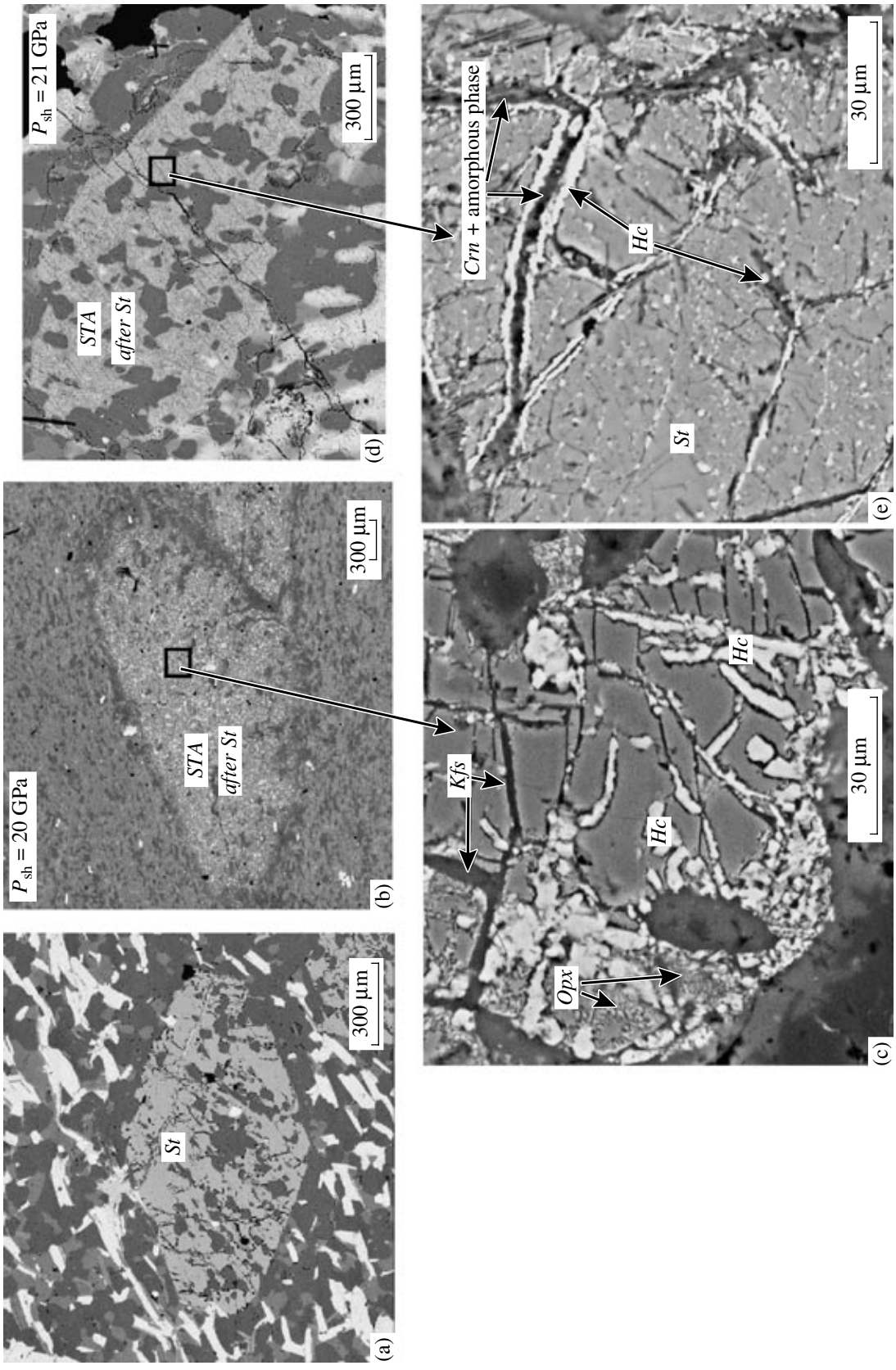

Fig. 4. Staurolite from (a) the unaltered target schist, (b, c) shock–thermal aggregate (STA) replacing staurolite in impacted schist from the Jänisjärvi astrobleme, and (d, e) schist affected by a shock wave in the experiment.

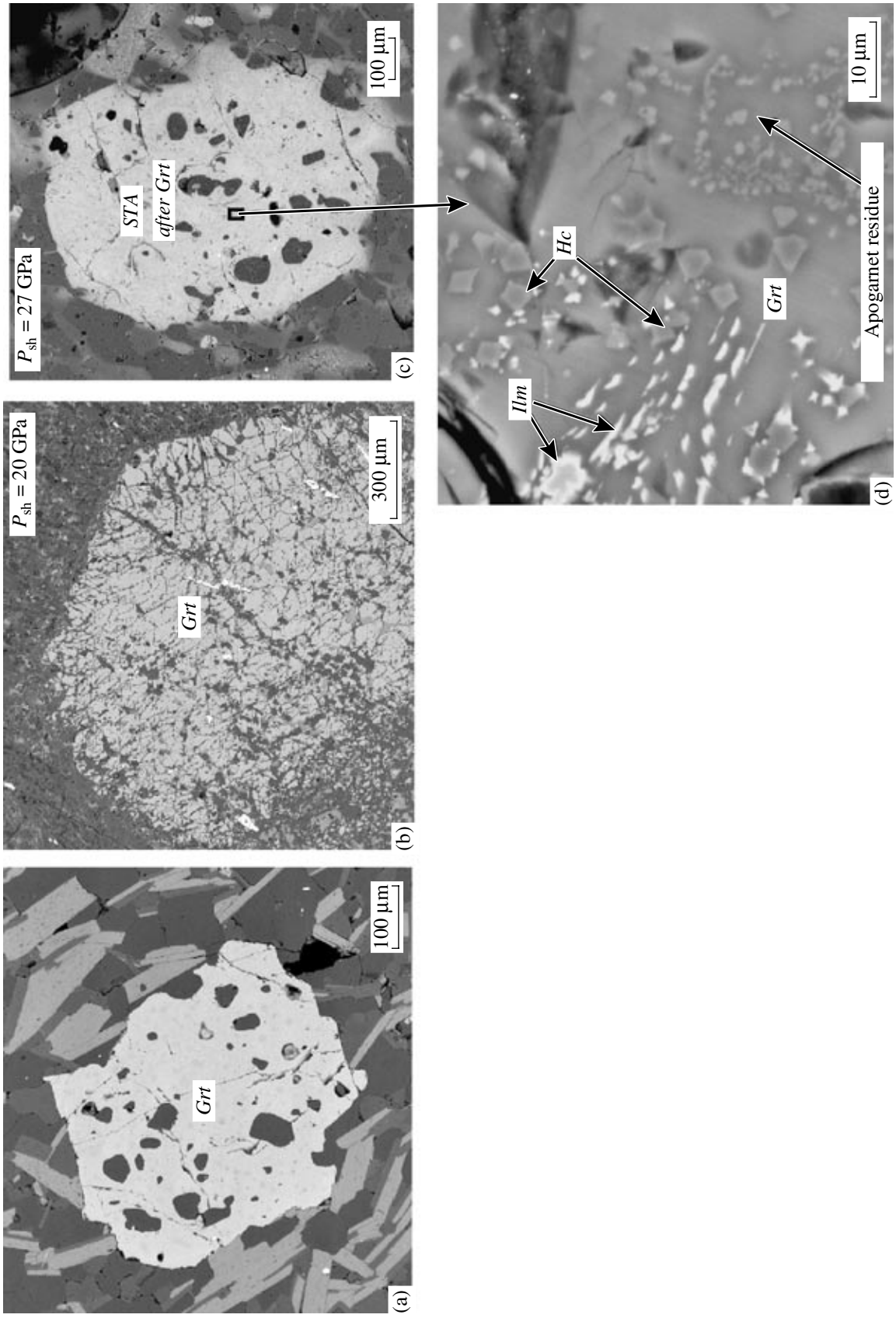

Fig. 5. Garnet from (a) the unaltered target schist, (b) impacted schist from the Jänisjärvi astrobleme, and (c, d) a shock–thermal aggregate replacing garnet in schist affected by a shock wave in the experiment.

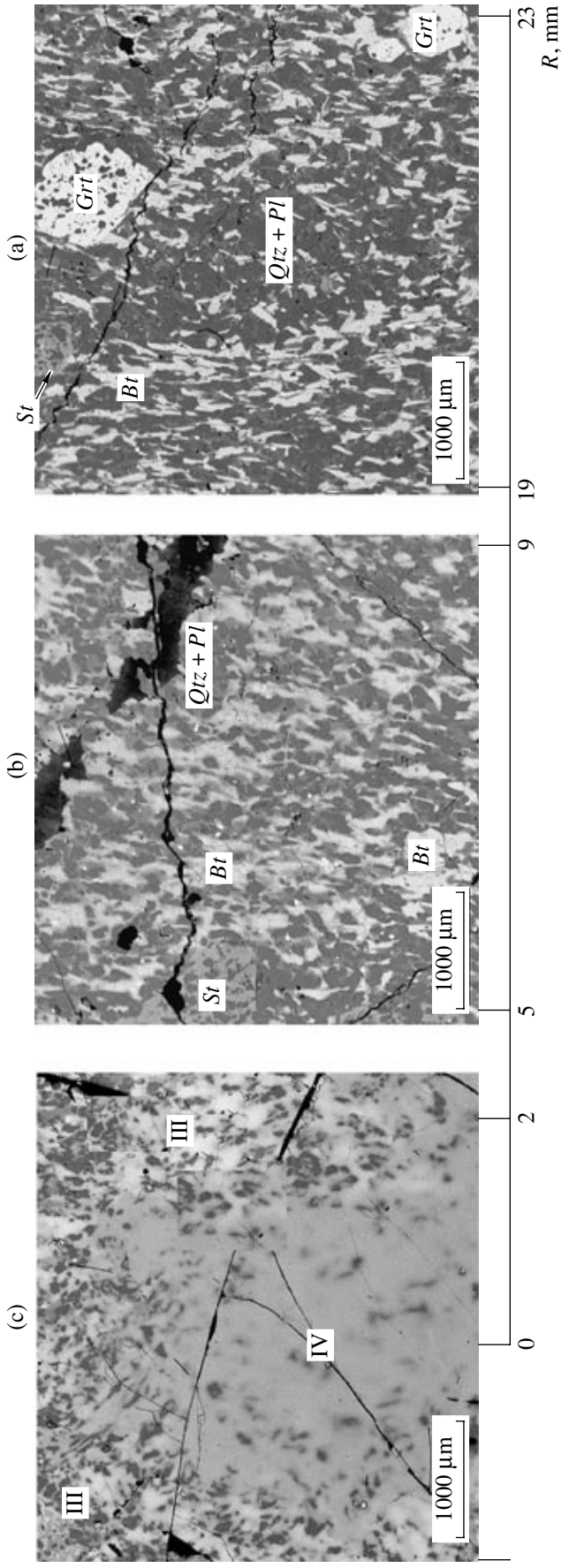

Fig. 6. Schist in discrete zones of the shock-loaded experimental rock sample.
(a) Zone I. The texture of the rock remains unmodified, the grain boundaries of minerals are sharp. (b) Zone II. The texture of the rock is generally preserved, but the boundaries of mineral grains are not as sharp and become diffuse. (c) Zone IV. Central zone of melting. The melts of all minerals mix. Darker patches in the light gray mass are quartz glass, which suggests that the melts do not homogenize completely. The transition to zone III is gradual. *R* is the radius of the sample sphere (in mm).

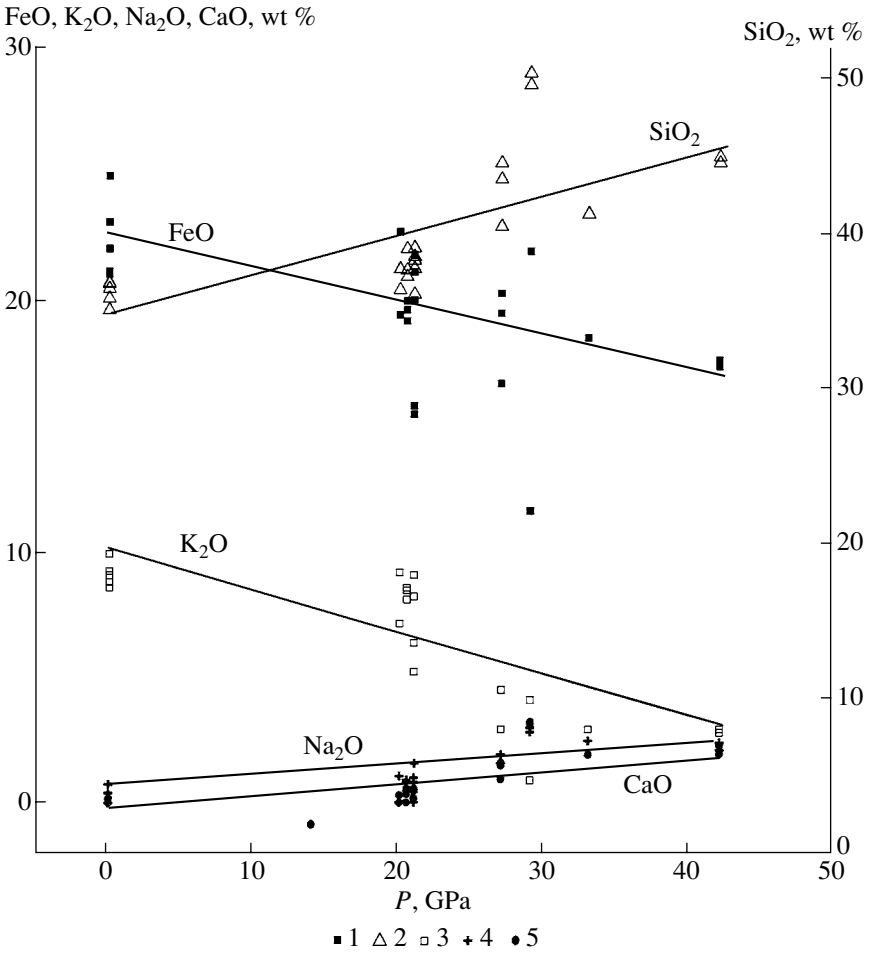

Fig. 7. Variations in the concentrations of FeO, SiO_2, K_2O, Na_2O, and CaO in biotite from schist in correlation with the shock pressure. (1) FeO, (2) SiO_2, (3) K_2O, (4) Na_2O, (5) CaO.

VOLNA computer program (Kuropatenko et al., 1989), which makes use of the Hugoniot adiabat (calculated from the density of the pristine rock and its chemical and modal composition; Telegin et al., 1980) and an equation of state in the form for limiting compression (Zababakhin, 1997). The calculations indicate that the shock pressure at the shock wave front at radii of R = 24–15 mm was within the range of 20–25 GPa and further increased from 30 GPa at R = 8 mm to 90 GPa at R = 3 mm. The calculated pressure at the front of the converging spherical shock wave at R = 1 mm reached ~3 Mbar. Starting at R = 15 mm, the dependence of the amplitude of the shock pressure P on the sphere radius has the form $P = 304.7R^{-1.1}$ GPa. Thus, the calculations indicate that the pressure on the rock at $R < 15$ mm at the shock wave front rapidly increased and reached a maximum at small radii due to the spherical geometry of the shock wave.

The rock temperature at the shock wave front was evaluated as proportional to the thermal constituent of the inner energy at a constant heat capacity. The latter condition leads to overestimated temperature values.

Zoning acquired by the sample after the passage of a spherical converging shock wave. After its shock-wave metamorphism, the sample displayed four zones, which were examined in a polished cross section of the sample (Figs. 6a–6c).

The outermost zone (zone I) is approximately 12.5 mm thick (between R = 24 mm and R ~ 11.5 mm of the sample). The texture of the rock is the same as the texture of the pristine (not metamorphosed by the shock wave) rock, with sharp boundaries between mineral grains (Fig. 6a). The pressures in this zones reached 25–20 GPa. The chemical alterations of minerals become discernible only in the part of the zone situated closer to the center of the sphere, at different distances from the center for each mineral, i.e., at different shock pressures.

The second zone (zone II) is 5–7 mm thick. The original texture of the rock is generally preserved, but the boundaries of mineral grains become diffuse (Fig. 6b) and not as sharp as in the previous zone owing to the migration of chemical components during the pressure pulse. The shock pressures in the inner portion

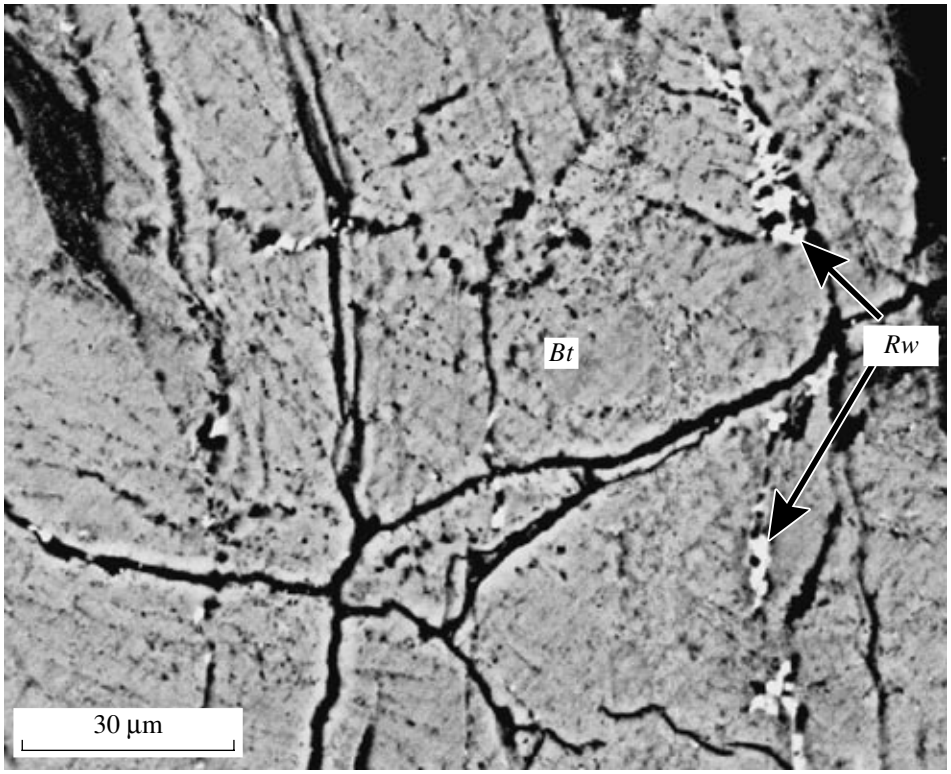

Fig. 8. Minute cracks in biotite filled with small ringwoodite grains.

of this zone reached 50 GPa. Zone II is characterized by widespread solid-phase alterations of minerals: amorphization of quartz and plagioclase, the development of shock thermal aggregates after biotite, garnet, and staurolite.

The third zone (zone III) had a width of 2–1.5 mm. The texture of the rock composing this zone was notably modified. The boundaries between mineral grains virtually disappeared, giving way to gradual transitions between mineral grains (Fig. 6c). This zone corresponded to the selective melting of minerals. The shock pressures in this zone ranged from 50 to 70–80 GPa at the outer to inner boundaries of the zone, respectively.

The fourth zone (zone IV) at the center of the sphere was 7–9 mm thick and was characterized by the complete melting of its material under pressures of >80 GPa. The boundary between zones III and IV was gradual, diffuse, and uneven, with the transition zone as thick as 100 μm. The melt in the zone was not completely homogenized, as can be seen in SEM images showing darker patches of quartz glass that did not mix with the rest of the melt (Fig. 6c).

It should be emphasized that the boundaries between the zones were drawn fairly arbitrarily, because the minerals composing these zones have different chemical compositions, crystal structures, and, as a consequence, analogous shock-induced features (such as amorphization, shock-induced thermal decomposition, and melting) appeared in them under different shock pressures.

Transformation of mineral chemistries under the effect of a shock wave. *Biotite* $K(Fe^{2+},Mg)_{3-x}(Al,Fe^{3+},Ti)_x[AlSi_3O_{10}](OH,F)_2$ is a phyllosilicate in which the apexes of the silicon–oxygen tetrahedra in neighboring two sheets face one another, and the sheets are connected through a sheet of octahedrally coordinated cations into a layer. These three-sheet (tetrahedral—octahedral—tetrahedral) layers are, in turn, connected through another set of cations. The interlayer K^+ cations are twelve-coordinated (coordination number $N = 12$). The Mg^{2+}, Fe^{2+}, Fe^{3+}, Ti, and part of the Al^{3+} cations compose octahedral layers and are six-coordinated ($N = 6$) with respect to oxygen: the N of Si and some Al^{3+} cations is equal to 4 (Godovikov, 1975).

When a spherical converging shock wave affects the mineral and $P \approx 20.5$ GPa, statistically significant K and Fe migration from its structure begins (Fig. 7, Table 1) (Kozlov et al., 2001, 2003). The removal of K ($N = 12$) is thereby more active than the removal of Fe ($N = 6$). At $P \approx 29$ GPa, these elements are joined by Mg ($N = 6$) (Table 1). At pressures above ~27 GPa, biotite starts to receive statistically significant amounts of Ca, Si, and Na (Fig. 7, Table 1).

Shock thermal aggregates appear already at pressures of 20–21 GPa at the shock wave front in the form of minute veinlets along small cracks (Fig. 8). The

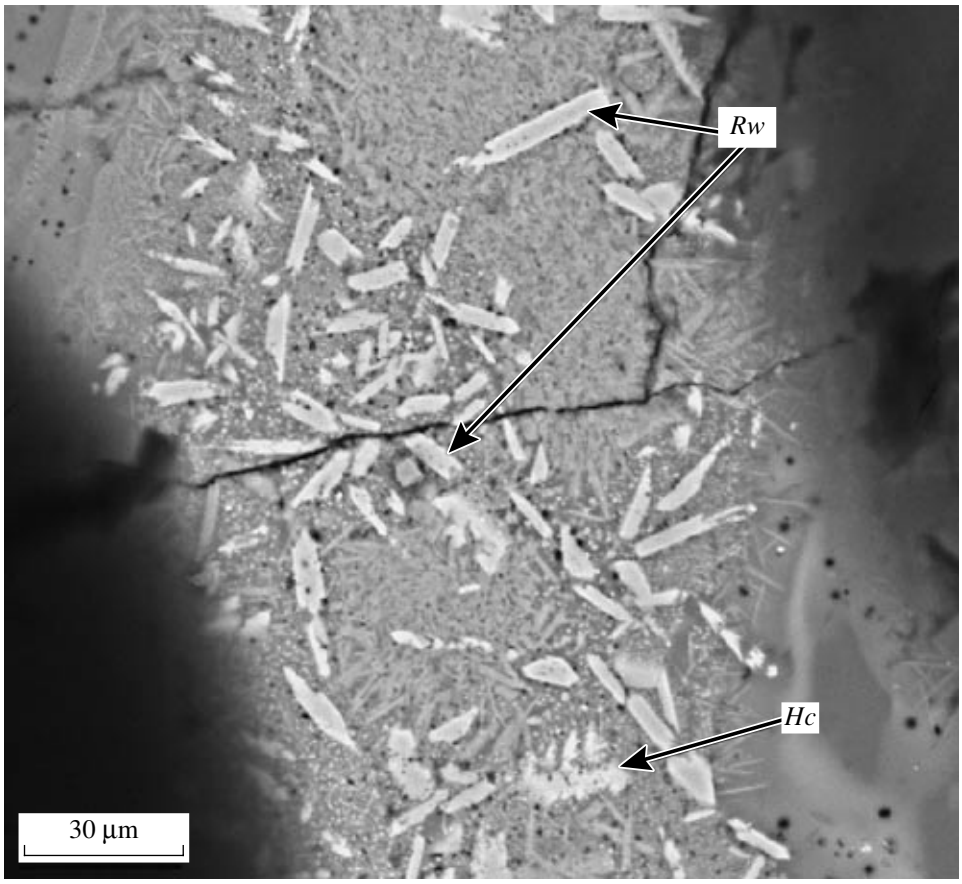

Fig. 9. Shock–thermal aggregate replacing biotite. The aggregate consists of tiny hercynite grains and elongated ringwoodite crystals submerged into an apobiotite residue (gray). $P_{sh} \approx 22$ GPa.

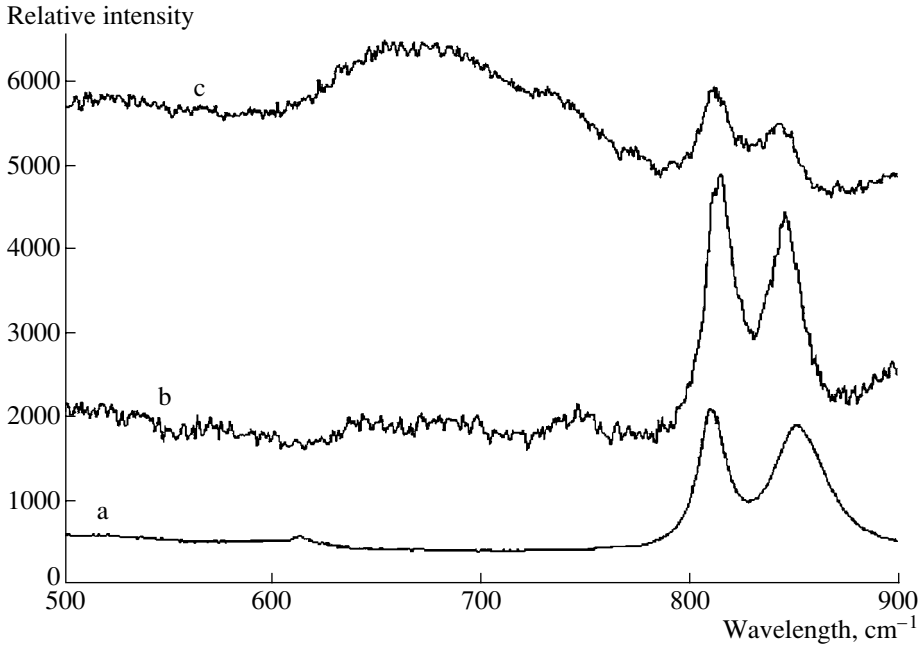

Fig. 10. Raman spectra (500–900 cm^{-1}). (a) Synthetic ringwoodite obtained under static conditions (see text); (b, c) spectra of aluminous ringwoodite produced in shock-loaded schist.

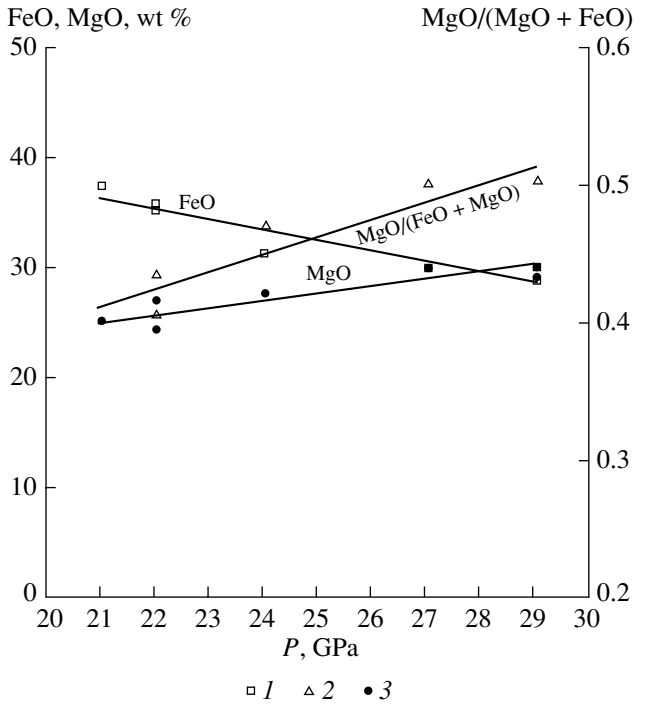

Fig. 11. Variations in the MgO/(MgO + FeO) ratio and the concentrations of FeO and MgO in aluminous ringwoodite as a function of the shock pressure. (*1*) FeO concentration; (*2*) MgO/(MgO + FeO) ratio; (*3*) MgO concentration.

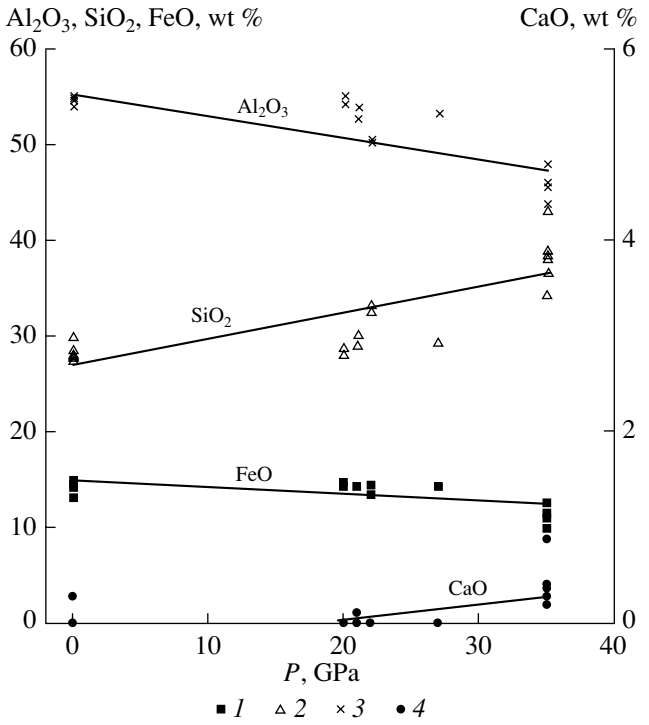

Fig. 12. Variations in the concentrations of FeO, SiO_2, Al_2O_3, and CaO in staurolite from the schist as a function of the shock pressure. (*1*) FeO; (*2*) SiO_2; (*3*) Al_2O_3; (*4*) CaO.

aggregates consist of ringwoodite and spinel of composition close to that of hercynite submerged in the apobiotite residual mass (Fig. 3a, Table 2). These aggregates were likely produced owing to drastic changes in the pressure along weakened zones, so-called adiabatic shear (Langenhorst and Poirier, 2000). In zone II, where the pressure at the shock wave front reached 25 GPa and more, the shock–thermal aggregates completely replaced biotite grains (Figs. 2c, 9). Ringwoodite occurs in these aggregates as small (no longer than 20 μm, occasionally up to 40 μm long and up to 7–8 μm wide) grains. The crystals are commonly platy, sometimes with hollow terminations (Fig. 9). As the shock pressures increased, the amount of ringwoodite in the shock-thermal aggregates after biotite increased (Sazonova et al., 2006), as also increased the elongation L (the length to width ratio) of the ringwoodite crystals. The dependence of the elongation L (μm) of ringwoodite crystals on the shock pressure P (GPa) is expressed by the equation $L = -20.5 + 1.1P$ at $S = 1.38$, $R = 0.885$, and $n = 36$, where S is the standard deviation, R is the correlation coefficient, and n is the number of measurements of elongation values at different pressures.

The identification of the mineral with ringwoodite was confirmed by Raman spectroscopy (Kozlov et al., 2002, 2003) (Fig. 10). The comparison of the Raman spectra of a ringwoodite standard and the spectra of this mineral from our sample indicates that the latter spectra have a high background, a feature suggesting that the mineral may contain much admixtures. This is corroborated by microprobe analyses of ringwoodite grains (Table 2). Our ringwoodite pervasively contains some components that are atypical of this mineral: Al, Ti, K, and sometimes Ca. These admixtures occur because this ringwoodite was produced via the decomposition of biotite, with some of its components (such as Si, Fe, and Mg) incorporated in ringwoodite and others (Al, K, and Ti) mostly removed or partly retained in the newly formed ringwoodite. The comparison of the compositions of the original biotite, ringwoodite, and the residue after biotite decomposition (Table 2) indicates that the removal of some components from the original mineral was associated with the addition of others: Na and Ca.

The statistical test of the dependence of the ringwoodite composition on the shock pressure points to a decrease in the FeO concentration and an increase in that of MgO and the MgO/(MgO + FeO) ratio (Fig. 11).

The scanning over areas within pseudomorphs after biotite revealed that an increase in the shock pressure was coupled with the enhancement of K and Fe removal from this mineral and K, Na, and Si introduction into it (Fig. 7, Table 1).

Staurolite $2(Al,Fe^{3+})_2[SiO_4]O \cdot Fe(OH)_2$ is a sublayer orthosilicate. Its structure includes chains of $[AlO_6]$ octahedra that are connected via $[AlO_6]$ octahe-

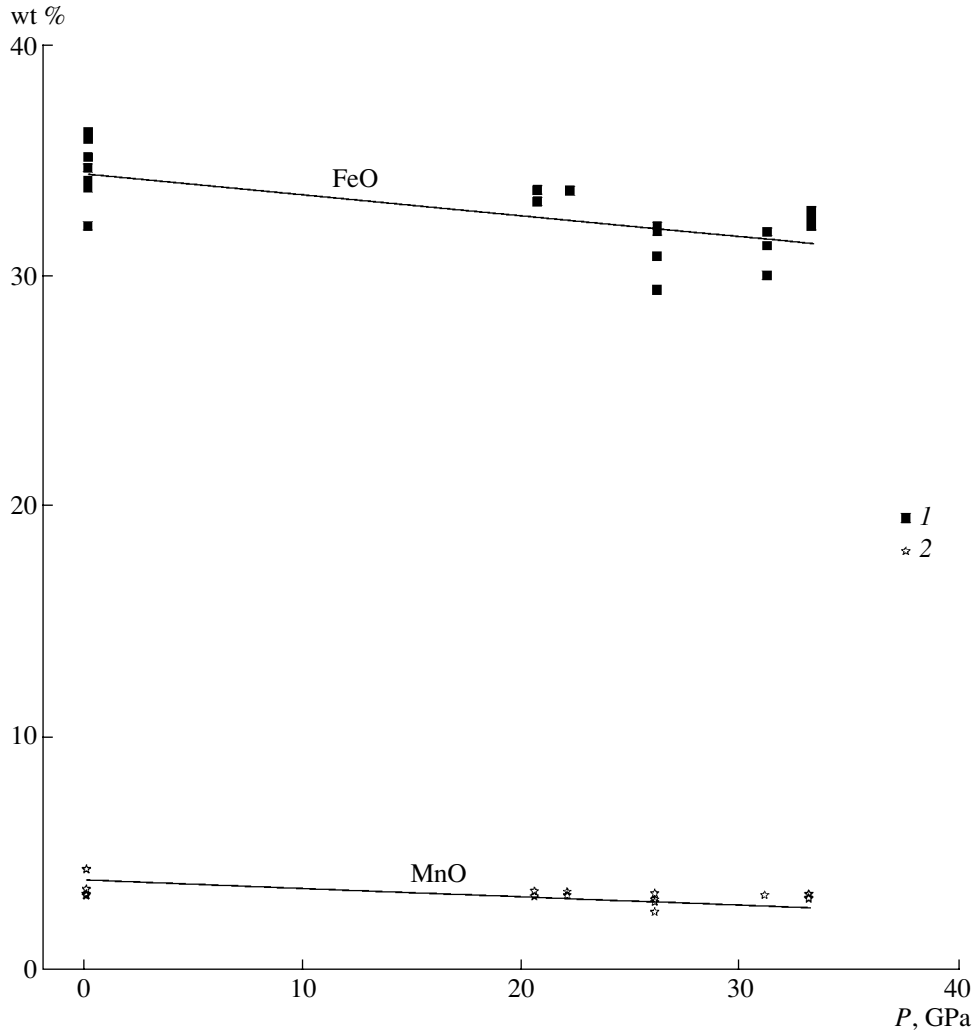

Fig. 13. Variations in the concentrations of FeO and MnO in garnet from the schist as a function of the shock pressure. (*1*) FeO; (*2*) MnO.

dra and $[SiO_4]$ tetrahedra with sheets of $[Fe(O,OH)_4]$ tetrahedra and $[AlO_6]$ octahedra with shared apexes. In the octahedra, Al can be partly substituted for Fe^{3+}, and, thus, Al and Fe^{3+} are six-coordinated by oxygen ions, and Si and Fe^{2+} are four-coordinated (Godovikov, 1975).

Already at pressures of ~20 GPa, elements octahedrally coordinated ($N = 6$) in this mineral (Fe and Al) start to migrate from it (Kozlov et al., 2001, 2003) (Table 3). The seemingly less active removal of Fe (more gently inclined plot in Fig. 12) than Al is explained by the fact that microprobe analyses give total Fe and, thus, involve both Fe^{3+} ($N = 6$) and Fe^{2+} ($N = 4$, this ion seems not to be prone to migrate). At $P \approx 36$ GPa, statistically significant introduction is also typical of Na (Table 3) and Ca (Fig. 12). The crystal structure of staurolite starts to decompose at $P \approx 21$ GPa into an aggregate of hercynite, corundum, and an apostaurolite residue (Figs. 3b, 4d, 4e; Table 4). The shock–thermal aggregates completely inherit their morphology and inner structure from the replaced mineral. At pressures higher than 36 GPa (Fig. 12, Table 3), microprobe scans over areas in pseudomorphs after staurolite yield elevated Si concentrations.

Garnet $(Fe^{2+},Mg,Mn,Ca)_3(Al,Fe^{3+},Ti)_2[SiO_4]_3$ is a subframe orthosilicate, whose structure can be imagined as a framework of $[SiO_4]$ tetrahedra, $[(Al,Fe^{3+},Ti)O_6]$ octahedra, and structural voids filled with $[(Fe^{2+},Mg,Mn,Ca)O_8]$ polyhedra. Larger ions (Fe^{2+}, Mg, Mn, and Ca) are eight-coordinated ($N = 8$) by oxygen ions, whereas smaller cations (Al, Fe^{3+}, and Ti) are six-coordinated ($N = 6$), and Si is four-coordinated (Godovikov, 1975). When the mineral is affected by a spherical converging wave at $P \approx 26$ GPa, it suffers the onset of Fe and Mn removal from it in statistically significant amounts (Table 5, Fig. 13), i.e., the unstable crystal-chemical site is that with $N = 8$ and, perhaps, also the site with $N = 6$ for Fe^{3+}. At $P \approx 26$–33 GPa, garnet undergoes shock–thermal decomposition into ilmenite, hercynite, and an apogarnet residue (Table 6,

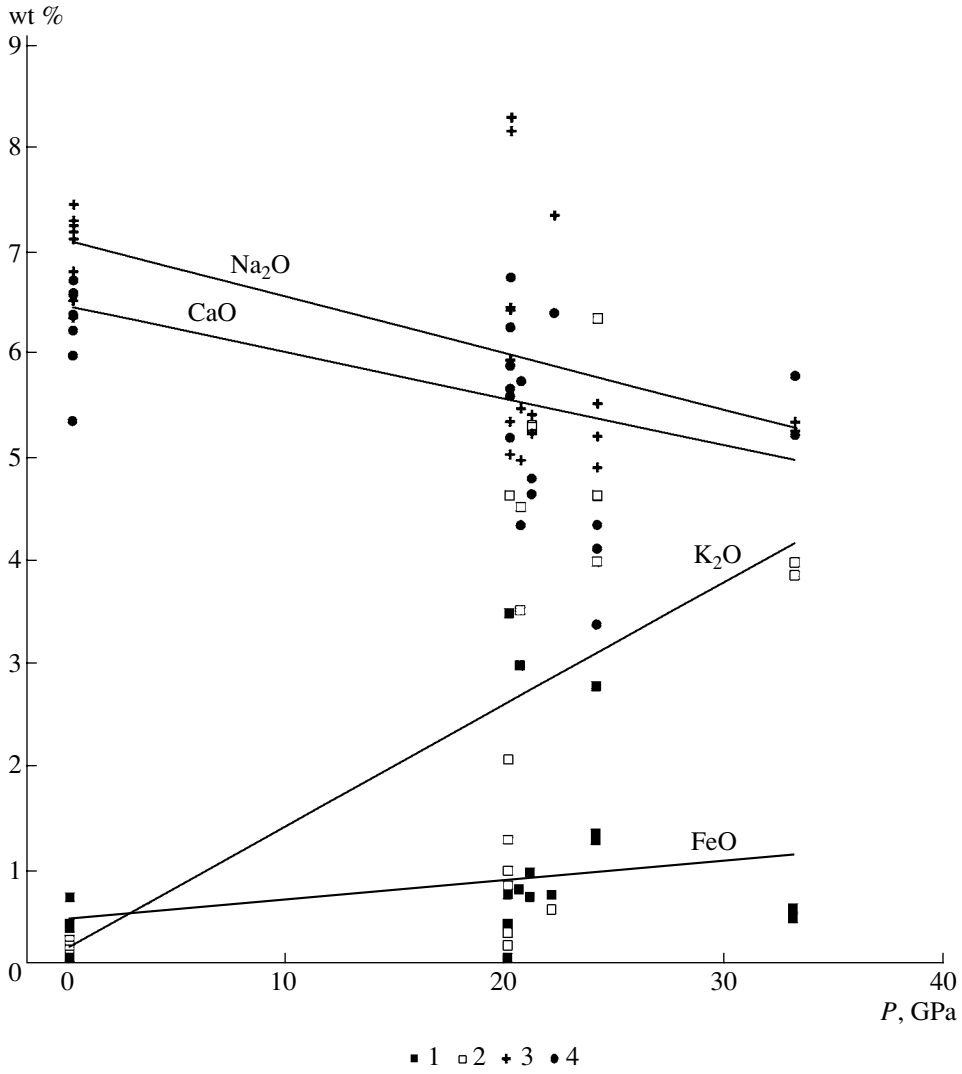

Fig. 14. Variations in the concentrations of K_2O, Na_2O, CaO, and FeO in plagioclase from the schist as a function of the shock pressure. (1) FeO; (2) K_2O; (3) Na_2O; (4) CaO. Straight lines demonstrate ranges with significant correlations between the concentrations and shock pressure.

Figs. 5c and 5d) (Kozlov et al., 2001, 2003). The shock–thermal aggregates completely preserve the morphology of the replaced mineral grains. Microprobe scanning over areas within pseudomorphs after garnet suggests that the only element removed from them is Fe (and minute amounts of Mn, Fig. 13), with the amounts of these removed elements increasing with increasing shock pressures.

Plagioclase $(Na_{1+x},Ca_{1-x})[(Si_{3-x},Al_{1+x})_4O_8]$ is a framework silicate with all tetrahedra sharing oxygen ions and thus forming a rigid three-dimensional structure. Some tetrahedra contain Al^{3+} in place of Si^{4+}, with interstices in the framework occupied by Na^+ and Ca^{2+} ions (Godovikov, 1975); Al and Si are four-coordinated, Ca is eight-coordinated, and Na is ten-coordinated by O ions.

At P = 20.5 GPa, Na and Ca start to migrate from this mineral in statistically significant amounts (Table 7, Fig. 14), whereas K and Fe are simultaneously introduced into it (Kozlov et al., 2001, 2003).

The migration of Na and Ca becomes more active with shock-wave pressures increasing to $P \approx 40$ GPa. Plagioclase is transformed into an amorphous phase (diaplectic glass of plagioclase composition) without its replacement by shock–thermal aggregates of newly formed minerals.

COMPARISON OF EXPERIMENTAL RESULTS AND NATURAL OBSERVATIONS

The succession of the shock–thermal decomposition of mafic minerals observed in nature is completely identical to that reproduced in our experiments. As was

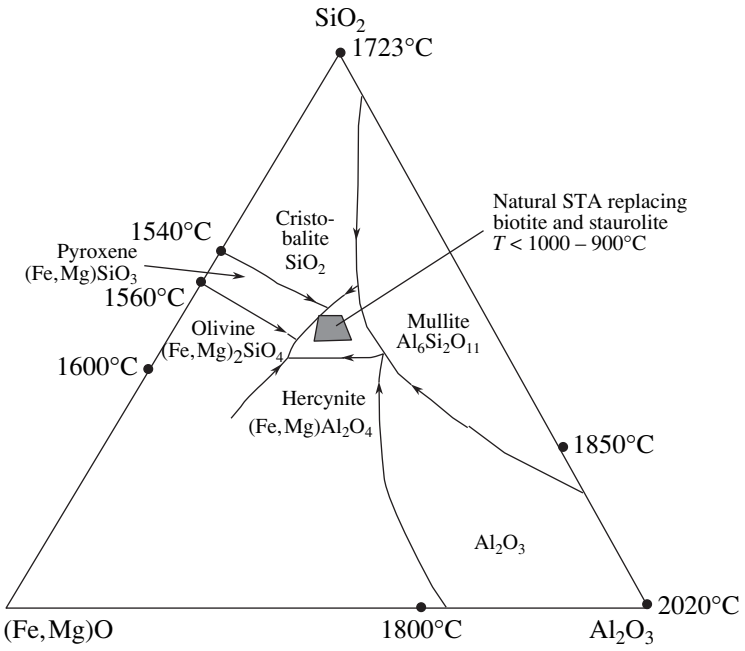

Fig. 15. Phase diagram for the SiO_2–Al_2O_3–(Fe,Mg)O system (Ehlers, 1972).

demonstrated by the results obtained by studying schist and breccia fragments from the Jänisjärvi astrobleme, the first alteration to occur in them is the shock–thermal decomposition of biotite (at ~20–22 GPa both in nature and in the experiments). The second mineral affected by this process is staurolite (at 20–25 GPa in nature and ~20 GPa in the experiments). Garnet from the Jänisjärvi astrobleme, whose shock pressures did not exceed 25 GPa, displays only evidence of the first stage of decomposition (see above), whereas this mineral from the Popigai astrobleme actively decomposed at shock pressures of 30 GPa and more (Sazonova et al., 1988; Fel'dman et al., 1990). In the experiments, shock–thermal aggregates after garnet developed within the pressure range of 26–33 GPa. At the same time, changes in the chemistry of all other minerals appear already at shock pressures lower than those at which new phases are formed.

Some differences in the composition of shock–thermal aggregates produced in nature and experiments can likely be accounted for, first of all, by the duration of the shock load, the volumes of the impacted rocks, the duration of their cooling after the effect of the shock wave, possibly, with different temperature regimes of the shock load. The diameter of the Jänisjärvi astrobleme is 280000 times greater than the diameter of our experimental sample. The duration of the shock load of the rock in the experiments was close to 2 μs, and the rock cooled in a chilling regime, i.e., very rapidly. A meteorite crater develops in several stages: (i) the shock compression of its rocks (a stage that lasts in a crater commensurable with the Jänisjärvi astrobleme for a few seconds) and (ii) excavation (a few dozen seconds) (*Impact Craters…*, 1983). The cooling of the impact material of large astroblemes, in which impact melts are produced, takes from a few hundreds to several thousand years (Simonds et al., 1978). These conditions are favorable for the annealing of the shock metamorphosed material and the transformations of its phases (first of all, those unstable under low pressures). For example, biotite in natural rocks is replaced by shock–thermal aggregates of orthopyroxene, ilmenite, potassic feldspar, and an amorphous mass. Experimental shock–thermal aggregates replacing biotite consist of aluminous ringwoodite, hercynite, and an apobiotite residue (Fig. 3). Judging from the SiO_2–Al_2O_3–FeO and SiO_2–Al_2O_3–MgO phase diagrams (Fig. 15, Ehlers, 1972), the temperature at which orthopyroxene started to crystallize was close to 1500°C. At the same time, the calculated crystallization temperature of aluminous ringwoodite in the shock–thermal aggregates after biotite in the experiments was 1060–1500°C.

Staurolite is in nature replaced by shock–thermal aggregates of orthopyroxene, hercynite, potassic feldspar, and an amorphous mass. The experimental shock–thermal aggregates replacing staurolite consist of corundum, hercynite, and an apostaurolite residue (Fig. 3). These differences suggest that the experimental temperatures were higher. As follows from the SiO_2–Al_2O_3–(Fe,Mg)O diagram (Fig. 15; Ehlers, 1972), corundum can crystallize at temperatures of 2000–1700°C, after which it is replaced by hercynite and mullite. In our experiments, the process terminated

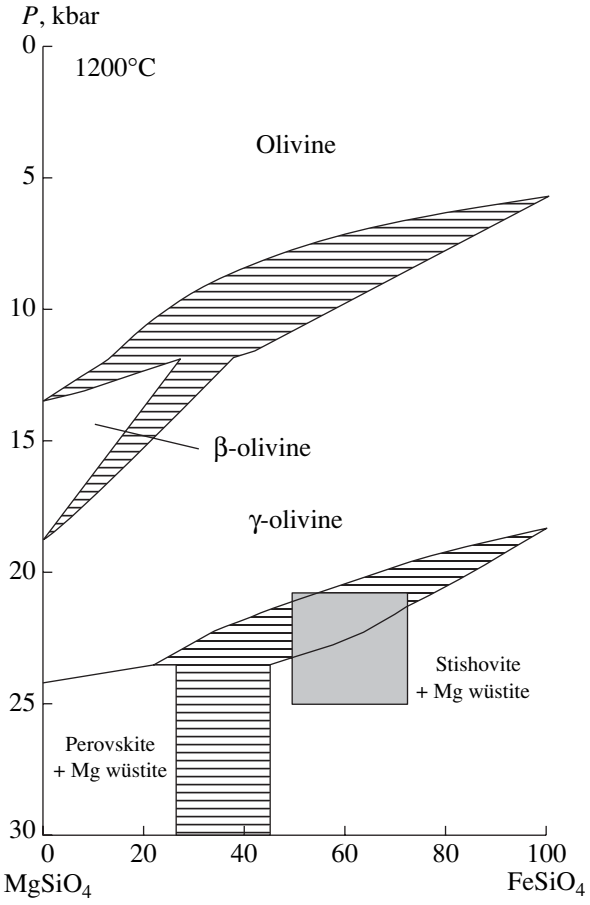

Fig. 16. Stability of olivine polymorphs (*Ultrahigh...*, 1998). The gray rectangle corresponds to the stability field of aluminous ringwoodite developing after biotite in our experiment. Hatched fields correspond to the coexistence of phases.

after the origin of corundum and hercynite (before the appearance of mullite), i.e., the temperature was no lower than 1700°C (Fig. 15).

As was mentioned above, garnet from the Jänisjärvi astrobleme, whose shock pressures did not exceed 25 GPa, shows no traces of chemical alteration. However, garnet from the impact rocks of the Popigai astrobleme (Sazonova et al., 1988), which had a composition close to that of the Jänisjärvi garnet, was partly replaced by shock–thermal aggregates. The latter developed at $P \geq 30$ GPa and consist of hercynite, orthopyroxene, potassic feldspar, and an apogarnet residue. The experimental shock–thermal aggregates developing after garnet consisted only of hercynite, ilmenite, and an apogarnet residue. The absence of potassic feldspar from the shock–thermal aggregates replacing garnet and staurolite in the experiments is likely explained by the rapid quenching of the rock at a higher temperature.

DISCUSSION OF OUR EXPERIMENTAL RESULTS

Ringwoodite. The occurrence of high-density polymorphic modifications of minerals is one of the most convincing indications of natural impact structures (meteorite craters or astroblemes). By the turn of this century, astroblemes have been determined to contain high-density polymorphs of silica (coesite and stishovite, carbon (diamond and lonsdaleite), and orthopyroxene (majorite). It was not until 2001 that γ-olivine (ringwoodite) was found in pumice from El Gasko, Extremadura, Spain (Diaz-Martinez et al., 2001). Our experiments were the first to synthesize ringwoodite under the effect of a shock wave on a plagioclase–quartz–biotite schist with garnet and staurolite (Kozlov et al., 2002, 2003; Sazonova et al., 2006).

Although the mineral contains notable amounts of foreign admixtures (Table 2), its composition is well approximated by the formula $(Fe, Mg)_2[(Si,Al)O_4]$. The high Al_2O_3 concentration (~14 wt %) in this mineral indicates that it should be referred to as aluminous ringwoodite. Its Fe/(FeO + MgO) ratio ranges from 0.5 to 0.73, and this mineral was formed in the experiment at $P_{sh} \approx 20$–30 GPa and $T \approx 1060$–1500°C, i.e., at higher *P–T* parameters (under a pressure roughly 1.5 times higher) than those of the static load (21–22 GPa at a comparable composition; *Ultrahigh-Pressure...*, 1998) (Fig. 16). The tendency toward higher *P–T* parameters of shock-wave metamorphism compared with metamorphism in a static regime is also well known for high-density polymorphs of silica (Mitsyuk et al., 1980) and carbon (Valter et al., 1992, Vishnevskii et al., 1997; Danilenko, 2003). The pressures under which polymorphic modifications are formed also depend on the mechanism of this process. The three currently known mechanisms able to produce polymorphs are crystallization from a melt, martensite transition in the solid state, and transition with the regrouping of ions with the removal and introduction of components (Fel'dman, 1990). Obviously, the processes that formed ringwoodite in our experiment belonged to the third type. This follows from the replacement of biotite by ringwoodite, i.e., a mineral of principally different composition. The migration of components in this process is readily seen from microprobe analyses of the original, intermediate, and final alteration products (see above). The mechanism that produced the ringwoodite is somewhat similar to the mechanism that formed diamond (togorite) in the Kara astrobleme (Ezerskii, 1982, 1986), whose shock pressures were ten times higher than the static pressure.

General tendencies in the mobility of major elements during shock metamorphism. The materials presented above suggest that the characteristics of the crystal structures of minerals are of principal importance for the amorphization of these minerals during

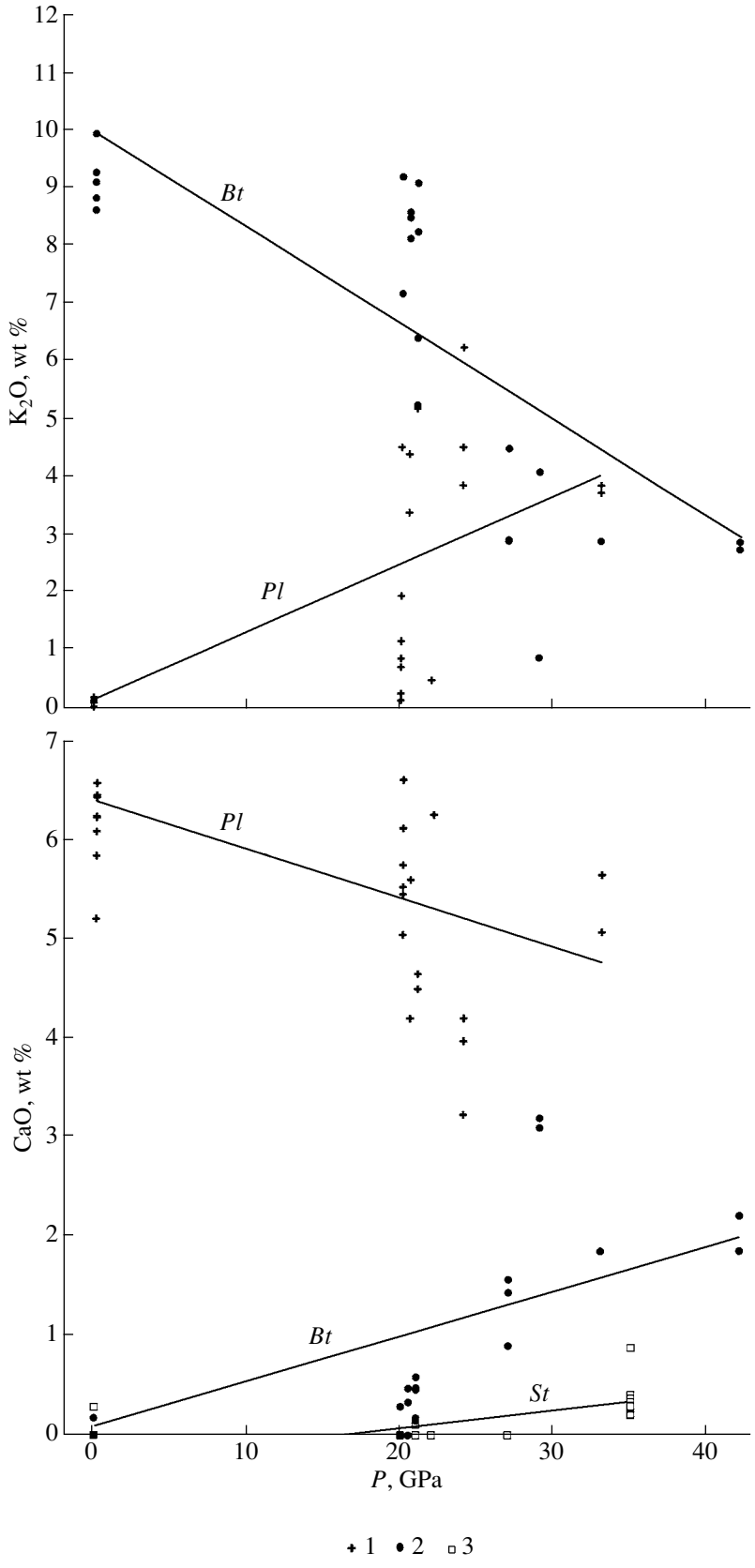

Fig. 17. Variations in the concentrations of K_2O and CaO in (1) plagioclase, (2) biotite, and (3) staurolite from the schist as a function of pressure at the shock wave front.

Table 1. Representative microprobe analyses (wt %) of biotite and shock–thermal aggregates replacing it (in correlation with the shock pressure)

Component	Spot analyses of biotite							Scanning over area within shock–thermal aggregates replacing biotite												
	Analysis number																			
	80238	80239	81243	81244	i134	54141	54140	1861	51194	51193	51192	2271	62158	1555	1554	1551	71205	71200	73207	74210
SiO_2	36.61	36.92	35.98	35.22	36.99	37.85	36.50	35.94	37.34	39.15	37.77	38.64	39.21	43.59	40.56	44.64	50.46	49.69	41.36	45.17
TiO_2	2.45	2.32	1.82	2.09	2.01	2.32	2.36	2.11	2.02	2.36	2.27	1.92	1.87	2.06	1.90	1.67	1.14	0.95	1.77	1.84
Al_2O_3	21.33	21.60	20.55	18.94	21.12	22.08	20.50	21.33	21.99	20.72	21.09	21.21	20.51	20.71	22.76	21.74	21.70	18.41	23.04	21.29
FeO	21.04	21.13	23.08	24.90	22.04	19.38	22.68	23.43	19.59	19.13	19.94	21.09	21.77	19.44	20.24	16.61	11.58	21.91	18.44	17.59
MgO	8.90	8.57	8.24	7.65	8.46	9.65	8.38	8.45	9.42	8.93	9.14	8.77	8.55	7.81	7.79	6.64	4.78	1.47	7.29	7.19
CaO	0.00	0.00	0.17	0.00	0.00	0.29	0.00	0.16	0.47	0.33	0.00	0.47	0.58	1.44	0.90	1.57	3.10	3.37	1.85	1.86
Na_2O	0.39	0.40	0.00	0.73	0.00	1.04	0.00	0.00	0.81	0.59	0.87	0.97	1.48	1.87	1.97	1.54	2.76	2.94	2.40	2.32
K_2O	8.79	8.58	9.23	9.91	9.06	7.14	9.16	8.23	8.08	8.44	8.54	6.36	5.21	2.87	2.89	4.46	4.06	0.85	2.87	2.73
Total	99.51	99.52	99.07	99.43	99.68	99.74	99.57	99.66	99.71	99.65	99.63	99.44	99.18	99.79	99.01	98.87	99.57	99.59	99.01	100.00
Number of cations per 24 oxygen ions																				
Si	5.80	5.81	5.79	5.78	5.86	5.87	5.84	5.74	5.84	6.09	5.93	6.00	6.09	6.54	6.14	6.64	7.26	7.40	6.21	6.69
Al(IV)	2.20	2.19	2.21	2.22	2.14	2.13	2.16	2.26	2.16	1.91	2.07	2.00	1.91	1.46	1.86	1.36	0.74	0.60	1.79	1.31
ΣSi + Al(IV)	8.00	8.00	8.00	8.00	8.00	8.00	8.00	8.00	8.00	8.00	8.00	8.00	8.00	8.00	8.00	8.00	8.00	8.00	8.00	8.00
Al(VI)	1.78	1.81	1.69	1.44	1.81	1.91	1.70	1.75	1.89	1.89	1.83	1.88	1.84	2.20	2.20	2.45	2.94	2.63	2.29	2.40
Ti	0.29	0.27	0.22	0.26	0.24	0.27	0.28	0.25	0.24	0.28	0.27	0.22	0.22	0.23	0.22	0.19	0.12	0.11	0.20	0.2
Fe^{2+}	2.79	2.78	3.11	3.42	2.92	2.51	3.03	3.13	2.56	2.49	2.62	2.74	2.83	2.44	2.56	2.07	1.39	2.73	2.32	2.18
Mg	2.10	2.01	1.98	1.87	2.00	2.23	2.00	2.01	2.19	2.07	2.14	2.03	1.98	1.75	1.76	1.47	1.03	0.33	1.63	1.59
Ca	0.00	0.00	0.03	0.00	0.00	0.05	0.00	0.03	0.08	0.05	0.00	0.08	0.10	0.23	0.15	0.25	0.48	0.54	0.30	0.30
Na	0.12	0.12	0.00	0.23	0.00	0.31	0.00	0.00	0.25	0.18	0.27	0.29	0.44	0.54	0.58	0.44	0.77	0.85	0.70	0.66
K	1.78	1.72	1.90	2.07	1.83	1.41	1.87	1.68	1.61	1.68	1.71	1.26	1.03	0.55	0.56	0.85	0.75	0.16	0.55	0.51
Σ cations	8.86	8.74	8.96	9.29	8.83	8.70	8.88	8.58	8.82	8.67	8.83	8.57	7.94	7.94	8.13	7.84	5.11	7.37	8.06	7.84
Distance from the center, mm	–	–	–	–	–	16.0	16.0	14.0	13.5	13.5	13.5	12	11.5	9.0	9.0	9.0	8.5	8.5	7.5	6.0
Shock pressure, GPa	0*	0	0	0	0	20	20	20	20	20	20	21	21	27	27	27	29	29	33	42

Note: Here and in Tables 2–7, shock pressure (0 GPa) are given for unaltered biotite from the host rocks.

Table 2. Chemical compositions (wt %) of unaltered biotite and the phases of shock–thermal aggregates replacing this mineral

Component	Unaltered *Bt*	Shock–thermal aggregate														
		Spl	Ringwoodite							Apobiotite residue						
	Analysis number															
	J134	2/47	2/29	2/30	59	72	74	J147	J168	2/31	60	73	J146	J148	J166	J167
SiO_2	36.99	0.41	33.83	32.95	33.16	34.08	30.64	33.76	32.57	45.08	44.81	40.69	39.37	41.79	46.45	45.57
TiO_2	2.01	0.48	0.44	0.43	0.27	0.20	0.27	0.33	0.39	2.66	2.87	2.71	2.6	1.58	2.38	2.14
Al_2O_3	21.12	60.01	6.01	8.55	6.62	3.40	8.95	3.09	7.80	25.96	27.55	23.69	21.83	26.55	25.81	26.64
FeO	22.04	22.82	29.73	28.87	29.82	35.21	35.67	37.41	31.29	15.34	12.9	16.27	17.9	15.89	12.36	12.37
MnO	0.00	0.00	0.00	0.00	0.00	0.00	0.00	0.00	0.00	0.28	0.00	0.00	0.00	0.00	0.00	0.00
MgO	8.46	14.54	29.77	29.07	30.03	27.10	24.38	25.20	27.71	3.74	3.15	7.26	8.46	5.41	2.75	3.06
CaO	0.00	0.00	0.00	0.00	0.00	0.00	0.00	0.00	0.12	1.20	0.59	0.37	0.55	1.21	1.06	1.58
Na_2O	0.00	0.00	0.00	0.00	0.00	0.00	0.00	0.00	0.00	1.59	2.58	1.10	1.14	1.86	3.45	3.71
K_2O	9.06	0	0.22	0.12	0.09	0.00	0.09	0.21	0.12	4	5.16	7.56	7.65	5.42	5.17	4.56
Total	99.68	98.26	100	100	100	100	100	100	100	99.85	99.61	99.65	99.5	99.71	99.43	99.63
Number of cations in the formulas of minerals																
Si	5.86	0.01	0.91	0.88	0.90	0.94	0.85	0.95	0.89							
Al(IV)	2.14	0.00	0.09	0.12	0.10	0.06	0.15	0.05	0.11							
Ti	0.24	0.01	0.01	0.01	0.01	0.00	0.01	0.01	0.01							
Al(VI)	1.81	1.88	0.10	0.15	0.11	0.06	0.15	0.05	0.13							
Fe^{2+}	2.92	0.46	0.67	0.65	0.67	0.82	0.83	0.88	0.71							
Mn	0	0.00	0.00	0.00	0.00	0.00	0.00	0.00	0.00							
Mg	2.00	0.58	1.20	1.16	1.21	1.12	1.01	1.05	1.12							
Ca	0.00	0.00	0.00	0.00	0.00	0.00	0.00	0.00	0.00							
Na	0.00	0.00	0.00	0.00	0.00	0.00	0.00	0.00	0.00							
K	1.83	0.00	0.01	0.00	0.00	0.00	0.00	0.01	0.00							
Distance from the center, mm	–	9.0	8.5	8.5	9.0	11.0	11.0	11.5	10.0	9.0	9.0	11.0	11.5	11.5	10.0	10.0
Shock pressure, GPa	0	27	29	29	27	22	22	22	25	27	27	22	21	21	25	25

Table 3. Representative microprobe analyses (wt %) of staurolite and shock–thermal aggregates replacing it (in correlation with the shock pressure)

Component	Spot analyses of staurolite									Scanning over area within shock–thermal aggregates replacing staurolite									
	Analysis number																		
	ST1	ST2	J130	J131	J135	J136	ST3	ST4	ST19	ST18	ST14	ST16	ST17	2/23	2/10	2/5	2/9	ST5	ST6	ST7
SiO_2	28.07	28.48	27.97	27.91	27.75	27.35	28.84	28.37	29.21	30.27	29.94	32.69	33.53	29.35	34.43	43.44	38.26	36.68	38.97	38.54
TiO_2	0.57	0.61	0.53	0.57	0.42	0.55	0.64	0.68	0.51	0.58	0.49	0.49	0.59	0.54	0.63	0.40	0.87	0.62	0.54	0.61
Al_2O_3	55.21	54.89	54.99	55.21	55.29	55.03	54.47	55.10	54.07	52.94	54.13	50.83	50.54	53.46	48.26	44.02	45.89	48.24	46.20	45.89
FeO	14.78	14.34	15.02	14.76	15.05	15.00	13.88	14.33	14.17	14.03	13.15	13.99	13.33	14.33	11.21	10.00	12.30	12.57	11.60	12.56
MnO	0.19	0.32	0	0.33	0	0.33	0.38	0	0.20	0	0.43	0.22	0.32	0	0	0	0	0	0.32	0.30
MgO	1.17	1.22	1.06	1.06	1.16	1.49	1.67	1.20	1.50	1.58	1.35	1.42	1.56	1.39	2.27	0.96	1.32	1.31	1.38	1.29
CaO	0	0	0	0	0	0	0	0	0	0.11	0.28	0	0	0	0.88	0.21	0.37	0.20	0.40	0.29
Na_2O	0	0	0	0	0	0	0	0	0	0	0	0	0	0	0.71	0	0.36	0	0.45	0.47
K_2O	0	0	0	0	0	0	0.09	0	0.14	0	0	0	0	0.12	1.27	0.13	0.21	0	0.14	0
Total	100	100	100	100	100	100	100	100	100	100	100	100	100	99.2	100	99.2	100	100	100	100
Number of cations per 24 oxygen ions																				
Si	3.99	4.05	3.99	3.98	3.96	3.91	4.09	4.03	4.15	4.29	4.23	4.62	4.71	4.17	4.84	5.93	5.32	5.11	5.59	5.36
Al(IV)	0.00	0.00	0.01	0.02	0.04	0.09	0.00	0.00	0.00	0.00	0.00	0.00	0.00	0.00	0.00	0.00	0.00	0.00	0.00	0.00
ΣSi + Al(IV)	3.99	4.05	4.00	4.00	4.00	4.00	4.09	4.03	4.15	4.29	4.23	4.62	4.71	4.17	4.84	5.93	5.32	5.11	5.59	5.36
Ti	0.06	0.06	0.06	0.06	0.04	0.06	0.07	0.07	0.05	0.06	0.05	0.05	0.06	0.06	0.07	0.04	0.09	0.07	0.06	0.06
Al(VI)	9.25	9.19	9.24	9.25	9.26	9.18	9.09	9.23	9.04	8.85	9.01	8.46	8.36	8.96	8.00	7.08	7.53	7.92	7.81	7.52
Fe^{2+}	1.76	1.70	1.79	1.76	1.80	1.79	1.64	1.70	1.68	1.66	1.55	1.65	1.56	1.70	1.32	1.14	1.43	1.46	1.39	1.46
Mn	0.02	0.04	0.00	0.04	0.00	0.04	0.05	0.00	0.02	0.00	0.05	0.03	0.04	0.00	0.00	0.00	0.00	0.00	0.04	0.04
Mg	0.25	0.26	0.22	0.22	0.25	0.32	0.35	0.25	0.32	0.33	0.28	0.30	0.33	0.29	0.48	0.19	0.27	0.27	0.30	0.27
Ca	0.00	0.00	0.00	0.00	0.00	0.00	0.00	0.00	0.00	0.02	0.04	0.00	0.00	0.00	0.13	0.03	0.05	0.03	0.06	0.04
Na	0.00	0.00	0.00	0.00	0.00	0.00	0.00	0.00	0.00	0.00	0.00	0.00	0.00	0.00	0.19	0.00	0.10	0.00	0.13	0.13
K	0.00	0.00	0.00	0.00	0.00	0.00	0.02	0.00	0.02	0.00	0.00	0.00	0.00	0.02	0.23	0.02	0.04	0.00	0.02	0.00
Σ cations	11.34	11.25	11.32	11.33	11.35	11.39	11.22	11.25	11.15	10.93	10.98	10.49	10.35	11.04	10.41	8.51	9.51	9.75	9.80	9.52
Distance from the center, mm	–	–	–	–	–	–	14	14	12	12	11	11	11	9	7	7	7	7	7	7
Shock pressure, GPa	0	0	0	0	0	0	20	20	21	21	22	22	22	27	35	35	35	35	35	35

Table 4. Chemical compositions (wt %) of unaltered staurolite and the phases of shock–thermal aggregates replacing this mineral

Component	Unaltered *St* from target rocks				Shock–thermal aggregate										
					Crn			*Hc*		Apostaurolite residue					
	Analysis number														
	J130	J131	J135	J136	2/1	2/3	2/11	2/22	68	2/10	2/18	2/25	2/27	2/5	2/9
SiO_2	27.97	27.91	27.75	27.35	2.28	5.64	0.30	3.14	6.71	34.43	43.61	34.29	46.13	43.44	38.26
TiO_2	0.53	0.57	0.42	0.55	0.00	0.19	0.00	0.00	0.17	0.63	0.32	0.53	0.58	0.40	0.87
Al_2O_3	54.99	55.21	55.29	55.03	96.31	92.08	98.71	65.92	58.96	48.26	39.94	53.70	40.35	44.02	45.89
FeO	15.02	14.76	15.05	15.00	1.10	1.61	0.68	26.80	29.02	11.21	13.72	9.87	9.37	10.00	12.30
MnO	0.00	0.33	0.00	0.33	0.00	0.00	0.00	0.00	0.00	0.00	0.30	0.00	0.30	0.00	0.00
MgO	1.06	1.06	1.16	1.49	0.00	0.00	0.00	3.57	4.56	2.27	1.11	0.78	0.78	0.96	1.32
CaO	0.00	0.00	0.00	0.00	0.00	0.00	0.00	0.00	0.00	0.88	0.14	0.00	0.97	0.21	0.37
Na_2O	0.00	0.00	0.00	0.00	0.00	0.00	0.00	0.00	0.00	0.71	0.45	0.41	0.96	0.00	0.36
K_2O	0.00	0.00	0.00	0.00	0.00	0.00	0.00	0.00	0.15	1.27	0.18	0.16	0.45	0.13	0.21
Total	99.57	99.84	99.67	99.75	99.68	99.52	99.70	99.43	99.56	99.66	99.75	99.73	99.87	99.15	99.58
Number of cations in the formulas of minerals															
Si	3.99	3.98	3.96	3.91	0.04	0.10	0.01	0.08	0.18						
Al	0.06	0.06	0.04	0.06	0.00	0.00	0.00	0.00	0.00						
Ti	9.25	9.27	9.30	9.27	1.94	1.85	1.98	2.06	1.86						
Fe^{2+}	1.79	1.76	1.80	1.79	0.02	0.02	0.01	0.60	0.65						
Mn	0.00	0.04	0.00	0.04	0	0	0	0.00	0.00						
Mg	0.22	0.22	0.25	0.32	0	0	0	0.14	0.18						
Ca	0	0	0	0	0	0	0	0	0						
Na	0	0	0	0	0	0	0	0	0						
K	0	0	0	0	0	0	0	0	0						
Distance from the center, mm	–	–	–	–	7	7	7	9	12	7	9	9	9	7	7
Shock pressure, GPa	0	0	0	0	35	35	35	27	21	35	27	27	27	35	35

their shock–thermal decomposition with the development of shock–thermal aggregates. The settings of ions in the lattice of a mineral predetermines the onset of their migration and the intensity of this process (Fel'dman et al., 2003).

At the first level of the crystal chemical control, the minerals of our rock can be subdivided into two major groups: (i) framework plagioclase and quartz, which undergo amorphization, and (ii) biotite (phyllosilicate), staurolite (subphyllosilicate), and garnet (a subframework silicate), which suffer shock–thermal decomposition. The shock–thermal aggregates completely inherit their morphologies and inner structures from the replaced mineral grains, for example, the poikiloblastic textures of staurolite (Fig. 4) and garnet (Fig. 5) grains. The newly formed shock–thermal aggregates consist of minerals stable under corresponding *P–T* conditions and a residual phase, whose composition is not unambiguously predetermined by that of the primary mineral (Fig. 3). The newly formed phases of shock–thermal aggregates contain certain components of the original mineral and are able to actively exchange components with the surrounding material. Because of this, the residual phase may be enriched in some components of nearby minerals.

The second level of the crystal chemical control determines the succession of the shock–thermal decomposition of minerals. As the shock pressure increases, this process involves biotite (a phyllosilicate), staurolite (subphyllosilicate), and garnet (subframework silicate). Shock–thermal decomposition affects first of all crystalline phases with the most heterogeneous crystal structures. The more homogeneous the structure of a mineral, the more resistant this min-

Table 5. Representative microprobe analyses (wt %) of garnet and shock–thermal aggregates replacing it (in correlation with the shock pressure)

Component	Spot analyses of garnet										Scanning over area within shock–thermal aggregates replacing garnet											
	Analysis number																					
	GR17	GR18	J126a	J127a	J128	J129	GR3	GR4	GR1	GR2	GR5	GR6	GR7	GR8	GR9	GR10	GR11	GR12	GR13*	GR14	GR15	GR16
SiO_2	36.54	36.97	36.53	35.99	36.49	35.78	36.92	37.67	37.37	37.23	38.18	35.60	39.41	37.26	40.38	38.27	38.64	39.87	37.53	39.53	37.17	38.64
Al_2O_3	21.15	21.08	20.93	20.68	20.90	20.82	21.22	20.98	21.22	20.91	17.21	19.87	21.52	19.28	19.19	20.95	21.01	21.17	21.50	20.62	23.18	21.30
FeO	34.11	33.81	34.66	35.89	35.12	36.22	33.20	33.69	33.67	33.67	31.94	32.14	30.85	29.37	32.18	31.89	31.30	30.01	32.80	32.31	32.40	32.15
MnO	3.48	3.41	3.29	4.36	3.26	4.33	3.39	3.17	3.27	3.36	3.28	3.03	2.92	2.49	3.24	3.21	3.29	3.15	3.26	3.09	3.03	3.23
MgO	2.58	2.59	2.48	1.66	2.48	1.23	2.80	2.42	2.80	2.35	2.44	2.68	2.50	4.05	2.21	2.15	2.08	2.19	2.49	2.56	2.57	2.66
CaO	1.86	1.73	1.79	1.30	1.75	1.31	1.95	1.94	1.54	1.91	3.07	2.54	2.17	2.27	1.68	1.69	1.88	1.90	1.63	1.53	1.37	1.45
Na_2O	0	0	0	0	0	0	0	0	0	0.53	0	0	0	0.90	0.74	1.29	1.26	1.11	0	0	0	0
K_2O	0	0	0	0	0	0	0	0	0	0	0	0	0	1.20	0	0.21	0.20	0.53	0	0	0	0
Total	99.73	99.60	99.68	99.88	100.00	99.69	99.47	99.86	99.86	99.96	96.13	95.86	99.37	97.10	99.62	99.65	99.65	99.93	99.21	99.63	99.73	99.42
Number of cations per 12 oxygen ions																						
Si	2.97	3.00	2.97	2.96	2.97	2.95	2.99	3.03	3.01	3.01	3.03	2.83	3.11	2.94	3.22	3.07	3.09	3.16	3.02	3.15	2.96	3.08
Al(IV)	0.03	0.00	0.03	0.04	0.03	0.05	0.01		0.00	0.00	0.00	0.17	0.00	0.06	0.00	0.00	0.00	0.00	0.00	0.00	0.04	0.00
ΣSi + Al(IV)	3.00	3.00	3.00	3.00	3.00	3.00	3.00	3.03	3.01	3.01	3.03	3.00	3.11	3.00	3.22	3.07	3.09	3.16	3.02	3.15	3.00	3.08
Al(VI)	1.99	2.01	1.98	1.96	1.97	1.97	2.00	1.99	2.01	1.99	1.61	1.69	2.00	1.73	1.80	1.98	1.98	1.97	2.04	1.94	2.14	2.00
Fe^{3+}	0.01	0.00	0.02	0.04	0.03	0.03	0.00	0.01	0.00	0.01	0.39	0.31	0.00	0.27	0.20	0.02	0.02	0.03	0.00	0.06	0.00	0.00
$\Sigma Ti + Al(VI) + Fe^{3+}$	2.00	2.01	2.00	2.00	2.00	2.00	2.00	2.00	2.01	2.00	2.00	2.00	2.00	2.02	2.00	2.00	2.00	2.00	2.04	2.00	2.14	2.00
Fe^{2+}	2.31	2.29	2.34	2.43	2.36	2.47	2.25	2.26	2.27	2.27	1.73	1.83	2.04	1.67	1.95	2.12	2.07	1.96	2.21	2.09	2.16	2.15
Mn	0.24	0.23	0.23	0.30	0.22	0.30	0.23	0.22	0.22	0.23	0.22	0.20	0.19	0.17	0.22	0.22	0.22	0.21	0.22	0.21	0.20	0.22
Mg	0.31	0.31	0.30	0.20	0.30	0.15	0.34	0.29	0.34	0.28	0.29	0.32	0.29	0.48	0.26	0.26	0.25	0.26	0.30	0.30	0.31	0.32
Ca	0.16	0.15	0.16	0.11	0.15	0.12	0.17	0.17	0.13	0.16	0.26	0.22	0.18	0.19	0.14	0.15	0.16	0.16	0.14	0.13	0.12	0.12
Na	0	0	0	0	0	0	0	0	0	0	0	0	0	0.14	0.11	0.20	0.20	0.17	0	0	0	0
K	0	0	0	0	0	0	0	0	0	0	0	0	0	0.12	0.00	0.02	0.02	0.05	0	0	0	0
Σ cations	3.02	2.99	3.02	3.05	3.04	3.04	2.99	2.93	2.96	3.03	2.50	2.57	2.71	2.77	2.69	2.96	2.92	2.81	2.87	2.73	2.79	2.80
Distance from the center, mm	–	–	–	–	–	–	13	13	11	11	9.5	9.5	9.5	9.5	9.5	8	8	8	7.5	7.5	7.5	7.5
Shock pressure, GPa	0	0	0	0	0	0	21	21	22	22	26	26	26	26	26	31	31	31	33	33	33	33

Table 6. Chemical compositions (wt %) of unaltered garnet and the phases of shock–thermal aggregates replacing this mineral

Component	Unaltered *Grt*				Shock–thermal aggregate						
					Ilm	*Hc*	Apogarnet residue				
	Analysis number										
	J127a	J128	J129	J126a	2/38	2/40	2/41	2/42	2/43	2/44	2/46
SiO_2	35.99	36.49	35.78	36.53	0.81	0.43	41.99	40.44	43.81	40.60	39.67
TiO_2	0.00	0.00	0.00	0.00	73.99	0.49	3.44	0.21	0.00	0.45	0.00
Al_2O_3	20.68	20.90	20.82	20.93	1.53	59.10	14.64	17.11	14.42	20.31	19.35
FeO	35.89	35.12	36.22	34.66	21.68	33.50	32.67	33.28	33.17	26.71	32.94
MnO	4.36	3.26	4.33	3.29	0.99	1.68	3.51	3.40	3.63	2.20	3.50
MgO	1.66	2.48	1.23	2.48	0.74	4.52	1.94	3.60	2.06	3.16	2.31
CaO	1.30	1.75	1.31	1.79	0.00	0.00	1.48	0.94	2.12	2.57	1.51
Na_2O	0.00	0.00	0.00	0.00	0.00	0.00	0.00	0.00	0.50	2.29	0.46
K_2O	0.00	0.00	0.00	0.00	0.00	0.00	0.00	0.80	0.00	1.59	0.00
Total	99.88	100.00	99.69	99.68	99.74	99.71	99.66	99.77	99.71	99.87	99.75
Number of cations in the formulas of minerals											
Si	2.96	2.97	2.95	2.97	0.02	0.02					
Al(IV)	0.00	0.00	0.00	0.00	0.04	1.96					
Ti	2.00	2.00	2.02	2.01	1.23	0.01					
Fe^{2+}	2.47	2.39	2.50	2.36	0.4	0.79					
Mn	0.30	0.22	0.30	0.23	0.02	0.04					
Mg	0.20	0.30	0.15	0.30	0.02	0.19					
Ca	0.11	0.15	0.12	0.16	0	0					
Na	0.00	0.00	0.00	0.00	0	0					
K	0.00	0.00	0.00	0.00	0	0					
Distance from the center, mm	–	–	–	–	27	27	27	27	27	27	27
Shock pressure, GPa	0	0	0	0	9	9	9	9	9	9	9

eral to thermal decomposition. Because of this, the shock pressures needed to induce the onset of decomposition increase with the transition from a layered aluminosilicate (biotite) to a subframework mineral (garnet) increase from approximately 20 to 30 GPa.

The third level of the crystal chemical control is determined by the coordination of an ion in the crystal structure. Four-coordinated ions do not start migrating until the onset of melting of the material. Ions with higher coordination numbers are able to migrate through solid minerals, with this process being the more active, the higher the coordination number *N* of these ions.

The behaviors of the migrating ions are different. Some of them are accommodated in the lattices of neighboring minerals, for example, K removed from biotite enters plagioclase (Fig. 17), along with some Fe, and Ca removed from plagioclase is partly incorporated in staurolite and biotite (Fig. 7), and the intense introduction and removal of components can be detected in the residual amorphous phase (Tables 2, 4, 6). Other components are retained (in statistically significant amounts) in certain minerals of shock–thermal aggregates in the rocks or are accommodated in the interstitial melt (during partial melting) and, eventually, in the melt of the complete-melting zone.

The intensity of component migration increases with increasing shock pressures (Fig. 17), as can be revealed during the statistical treatment of data on the variations in the contents of components in the same minerals at different distances from the center of the experimental rock sphere (Fel'dman et al., 2003; Kozlov et al., 2003, 2004; Feldman et al., 1997). The intensity of migration in the outermost zone (zone I)

Table 7. Representative microprobe analyses (wt %) of plagioclase (in correlation with the shock pressure)

Component	Analysis number											
	80241	81245	81246	81247	J132	J133	J137	J138	80240	52195	52196	48161
SiO_2	60.54	61.19	61.87	61.49	61.11	61.42	61.16	61.45	60.72	59.16	60.61	60.95
Al_2O_3	25.52	24.75	24.32	24.91	24.98	25.15	25.06	24.51	24.64	23.37	24.59	24.36
FeO	0	0.58	0	0.325	0	0	0.29	0.29	0.61	3.34	0	0.61
MgO	0	0	0	0	0	0	0	0	0	0.384	0	0
CaO	7.05	6.08	5.83	6.23	6.57	6.44	6.22	6.42	6.25	6.11	5.52	6.60
Na_2O	6.37	6.97	7.30	6.73	7.04	6.65	7.10	7.15	7.16	5.51	8.15	6.30
K_2O	0	0	0.17	0.12	0.08	0	0.08	0	0.46	1.92	0.84	1.14
Total	99.48	99.56	99.49	99.80	99.77	99.67	99.91	99.81	99.84	99.79	99.71	99.95
Number of cations per 8 oxygen ions												
Si	2.68	2.71	2.74	2.72	2.71	2.72	2.71	2.73	2.71	2.69	2.71	2.72
Al(IV)	1.33	1.29	1.27	1.30	1.31	1.31	1.31	1.28	1.29	1.25	1.30	1.28
ΣSi + Al(IV)	4.02	4.01	4.01	4.03	4.02	4.03	4.02	4.01	4.00	3.94	4.00	4.00
Fe^{2+}	0	0.02	0	0.01	0	0	0.01	0.01	0.02	0.13	0	0.02
Mg	0	0	0	0	0	0	0	0	0	0.03	0	0
Ca	0.33	0.29	0.28	0.30	0.31	0.31	0.30	0.31	0.30	0.30	0.26	0.32
Na	0.55	0.60	0.63	0.58	0.61	0.57	0.61	0.61	0.62	0.49	0.71	0.54
K	0	0	0.01	0.01	0	0	0	0	0.03	0.11	0.05	0.06
Σ cations	0.88	0.91	0.91	0.89	0.92	0.88	0.92	0.93	0.97	1.05	1.02	0.95
Distance from the center, mm	–	–	–	–	–	–	–	–	–	14	14	14
Shock pressure, GPa	0	0	0	0	0	0	0	0	0	20	20	20

Component	Analysis number												
	48164	48165	54143	54144	62154	62156	57187	57188	66179	68170	68173	73206	73209
SiO_2	61.27	60.34	61.88	62.43	59.88	59.90	59.13	60.33	59.51	59.57	59.87	60.13	59.97
Al_2O_3	24.67	24.32	24.88	25.75	23.99	24.53	25.21	23.27	24.03	24.41	23.97	24.57	24.64
FeO	0.00	0.33	0	0	0.83	0.59	0.66	2.83	2.63	1.76	1.13	0.48	0.38
MgO	0	0	0	0	0	0	0	0.585	0.58	0.554	0	0	0
CaO	5.74	5.45	6.60	5.04	4.65	4.49	5.59	4.19	3.97	4.47	3.23	5.07	5.64
Na_2O	8.02	4.88	6.28	5.79	5.26	5.08	4.82	5.33	5.37	4.75	5.05	5.38	5.11
K_2O	0.24	4.48	0.12	0.69	5.14	5.16	4.37	3.37	3.84	4.48	6.52	3.83	3.71
Total	99.93	99.79	99.76	99.70	99.75	99.75	99.78	99.89	99.93	100.00	99.77	99.46	99.44
Number of cations per 8 oxygen ions													
Si	2.72	2.72	2.74	2.75	2.72	2.71	2.67	2.73	2.70	2.69	2.73	2.71	2.70
Al(IV)	1.29	1.29	1.30	1.34	1.28	1.31	1.34	1.24	1.28	1.30	1.29	1.30	1.30
ΣSi + Al(IV)	4.01	4.01	4.03	4.08	4.00	4.02	4.01	3.97	3.98	4.00	4.02	4.02	4.00
Fe^{2+}	0	0.01	0	0	0.03	0.02	0.02	0.11	0.10	0.07	0.04	0.02	0.01
Mg	0	0	0	0	0	0	0	0.04	0.04	0.04	0	0	0
Ca	0.27	0.26	0.31	0.24	0.23	0.22	0.27	0.20	0.19	0.22	0.16	0.24	0.27
Na	0.69	0.43	0.54	0.49	0.46	0.45	0.42	0.47	0.47	0.42	0.45	0.47	0.45
K	0.01	0.26	0.01	0.04	0.30	0.30	0.25	0.19	0.22	0.26	0.38	0.22	0.21
Σ cations	0.98	0.96	0.86	0.77	1.02	0.98	0.97	1.01	1.02	1.00	1.03	0.95	0.94
Distance from the center, mm	14	14	16	16	12	12	13	13	10	10	10	7.5	7.5
Shock pressure, GPa	20	20	20	20	21	21	21	21	24	24	24	33	33

increases relatively weakly, and the dispersions of the concentrations are generally insignificant. With the transition to zone II, whose material undergoes amorphization or shock–thermal decomposition, the intensity of migration drastically increases, as does the dispersion of the concentrations of compositions, i.e., the stoichiometric proportions of cations in minerals are distorted.

CONCLUSIONS

The following conclusions were drawn in the course of this research.

1. The differences between naturally occurring and experimentally produced shock–thermal aggregates seem to be explained by the more rapid cooling of the rock in the experiment because of the much smaller volume of the impacted rock and, consequently, its faster quenching.

2. Our experiments on the loading of rocks with shock waves were the first to produce ringwoodite, which was rich in Al_2O_3 and should be referred to as aluminous ringwoodite. The mineral was produced not by the martensite transition of olivine but by the replacement of a mineral phase of different composition (biotite) coupled with the migration of elements.

3. The characteristics of the crystal structure of a mineral are crucial for the transformations of this mineral by shock waves (amorphization or shock–thermal decomposition with the development of shock–thermal aggregates). The setting of ions in the crystal structure of a mineral controls the onset of their migration and the intensity of this process.

ACKNOWLEDGMENTS

The authors thank G.V. Kovalenko and G.G. Bondarchuk (Russian Federal Center for Nuclear Research—Zababakhin Institute of Technical Physics) for help with thermodynamic calculations. P.S. De Carli (SRI International, United States) is thanked for the sympathetic and fruitful discussion of the text of the manuscript and problems discussed in it. Our fieldwork at the Jänisjärvi astrobleme and the petrological study of the materials were financially supported by the Russian Foundation for Basic Research (project nos. 03-05-64496 and 05-05-64778) and a grant from the President of the Russian Federation for the support of leading research schools (Grant VNSH-1645.2003.5).

REFERENCES

1. V. V. Danilenko, *Synthesis and Agglomeration of Diamond by Detonation* (Energoatomizdat, Moscow, 2003) [in Russian].
2. A. Deutsch, F. Langenhorst, and V. Masaitis, "Mineralogy of Astroblemes—Terrestrial Impact Craters," in *Advanced Mineralogy*, Ed. by A. S. Marfunin (Springer-Verlag, Berlin, 1998), Vol. 3, 76–139.
3. E. Diaz-Martinez, E. Sanz-Rubio, C. Fernandez, and J. Martinez-Frias, "Evidence for a Small Meteorite Impact in Extremadura (W. Spain)," in *Proceedings of 6th European Science Foundation, Impact Workshop on Impact Markers in the Stratigraphic Record, Granada, Spain, 2001* (Granada, 2001), pp. 21–22.
4. E. G. Ehlers, *The Interpretation of Geological Phase Diagrams* (Freeman, San Francisco, 1972).
5. V. A. Ezerskii, "Ultrahigh-Pressure Polymorphs Produced by the Impact Transformation of Coals," Zap. Vseross. Mineral. O–va, No. 1, 26–33 (1986).
6. V. A. Ezerskii, "Shock-Metamorphosed Coal Matter in Impactites," Meteoritika, No. 41, 131–140 (1982).
7. V. I. Fel'dman and L. V. Sazonova, "Diaplectic Transformations of Mafic Minerals," Vestn. Mosk. Univ., Ser. 4: Geol., No. 5, 29–37 (1988).
8. V. I. Fel'dman, *Petrology of Impactites* (Mosk. Gos. Univ., Moscow, 1990) [in Russian].
9. V. I. Fel'dman, L. V. Sazonova, E. A. Kozlov, and Yu. N. Zhugin, "Migration of Some Chemical Elements in Spherical Stress Waves," in *Proceedings of 28th Lunar and Planetary Science Conference, Houston, USA, 1997* (Lunar. Planet. Inst., Houston, 1997), pp. 351–352.
10. V. I. Fel'dman, L. V. Sazonova, and A. V. Guzhova, "Biotite Transformations during Shock Metamorphism," Meteoritika, No. 47, 197–206 (1988).
11. V. I. Fel'dman, L. V. Sazonova, and E. A. Kozlov, "Mobility of Major Rock-Forming Elements during Shock Metamorphism: Experimental Evidence," Dokl. Akad. Nauk **393** (1), 1–3 (2003) [Dokl. Earth Sci. **393A** (9), 1033 (2003)].
12. V. I. Fel'dman, L. V. Sazonova, N. N. Kononkova, and D. Erg, "Diaplectic Transformations of Some Rock-Forming Minerals," Geokhimiya, No. 11, 1615–1620 (1987).
13. V. I. Fel'dman, L. V. Sazonova, and S. L. Kotel'nikov, "Distribution of the Shock Pressure in the Rocks of the Vorotilov Hole, Puchezh-Katunki Astrobleme," Dokl. Akad. Nauk **39** (5), 658–660 (1996) [Dokl. Earth Sci. **349A** (6), 936 (1996)].
14. V. I. Feldman, "The Conditions of Shock Metamorphism," in *Large Meteorite Impacts and Planetary Evolution*, Ed. by B. O. Dressler, R. A. F. Grieve, and V. L. Sharpton, Geol. Soc. Amer. Spec. Pap. **293**, 121–132 (1994).
15. *Geology of Astroblemes* (Nedra, Leningrad, 1980) [in Russian].
16. A. A. Godovikov, *Mineralogy* (Nedra, Moscow, 1975) [in Russian].
17. L. B. Granovsky, V. I. Feldman, N. N. Nikishina, et al., "A Study of Biotites from Allogene Breccia of Impact Crater Janisjarvi," in *Proceedings of 10th Lunar and Planetary Science Conference, Houston, USA, 1978* (Lunar. Planet. Inst., Houston, 1978), pp. 121–122.
18. R. Grieve and P. Robertson, "Variations in Shock Deformation at the Slate Islands Impact Structure, Lake Superior," Contrib. Mineral. Petrol. **58** (1), 37–51 (1976).
19. *Impactites* (Mosk. Gos. Univ., Moscow, 1981) [in Russian].
20. *Impact Craters at the Moon and Planets*, Ed. by M. A. Sadovskii (Nauka, Moscow, 1983) [in Russian].

21. E. A. Kozlov, "Investigations of Metals, Minerals, and Meteorites in Spherical Shock–Isoenthropic Experiments: Polymorphous and Phase Transformations, Shear and Strike-Slip Deformations, Physicochemical Transformations: A Review, in *Proceedings of International Conference of 5th Zababakhin Scientific Talks, Snezhinsk, Russia, 1999* (Ross. Fed. Yad. Tcenter–Nauch–Islled. Inst. Techn. Phys., Snezhinsk, 1999), pt. 1, pp. 579–590 [in Russian].

22. E. A. Kozlov, L. V. Sazonova, V. I. Fel'dman, et al., "Formation of Ringwoodite in High-Explosive Experiments on Muscovite–Biotite–Quartz States," in *Bayerisches Forschungsinstitut für Experimentelle Geochemie und Geophysik Universität Bayreuth, Annual Report* (Jahresbericht, 2002), pp. 100–101.

23. E. A. Kozlov, L. V. Sazonova, V. I. Fel'dman, et al., "Formation of Ringwoodite during Shock-Wave Loading of Two-Mica Quartz Schist: Experimental Data," Dokl. Akad. Nauk **390** (3), 379–381 (2003) [Dokl. Earth Sci. **390** (4), 571 (2003)].

24. E. A. Kozlov, L. V. Sazonova, and V. I. Fel'dman, "Crystallochemical Structure of Rock-Forming Minerals and Peculiarities, Sequence and Completeness of Physicochemical Transformations in Weak and Strong Shock Waves," in *Proceedings of 5th International Symposium on High Dynamic Pressures, Saint Malo, France, 2003* (Saint Malo, 2003), Vol. 1, 389–397.

25. E. A. Kozlov, V. I. Fel'dman, and L. V. Sazonova, "Crystallochemical Structure of Rock-Forming Minerals and Peculiarities, Sequence and Completeness of Physicochemical Transformations in Weak and Strong Shock Waves," in *Shock Compression of Condensed Matter—2003*, Ed. by M. D. Furnish, Y. M. Gupta, and J. W. Forbes (Am. Inst. Phys., 2004), pp. 1458–1461.

26. E. A. Kozlov, Yu. N. Zhugin, B. V. Litvinov, et al., "Phase Transformations of Wollastonite in Spherical Stress Waves," Dokl. Akad. Nauk **355** (3), 328–332 (1997).

27. E. A. Kozlov, Yu. N. Zhugin, B. V. Litvinov, et al., "Chemical Changes in Minerals Under Shock-Wave Loadings," Preprint of RFYaTs–VNIITF, Snezhinsk, 1998, no. 151.

28. E. A. Kozlov, Yu. N. Zhugin, L. V. Sazonova, and V. I. Fel'dman, "Migration of Chemical Components of Minerals under Shock-Wave Loading of Jänisjärvy Astrobleme Target Rocks (Karelia, Russia)," in *Proceedings of the 6th International Conference of Zababakhin Scientific Talks, Snezhinsk, Russia, 2001* (Russ. Fed. Nucl. Center–Research Inst. Techn. Phys., Snezhinsk, 2001), pp. 173–174 [in Russian].

29. V. F. Kuropatenko, G. V. Kovalenko, V. I. Kuznetsov, et al., "VOLNA Package and a Heterogeneous Differential Method for the Calculation of the Movement of Compressible Medium," in *Problems of the Atomic Science and Techniques (VANT). Series: Methods and Programs of Numerical Simulation of the Problems of Mathematical Physics*, No. 2, 9–25 (1989).

30. F. Langenhorst and J.-P. Poirier, "Anatomy of Black Veins in Zagami: Clues to the Formation of High-Pressure Phases," Earth Planet. Sci. Lett. **184** (1), 37–55 (2000).

31. B. V. Litvinov, E. A. Kozlov, Yu. N. Zhugin, et al., "On New Experimental Facilities for Studying Polymorphous and Phase Transitions, Solid-Phase Chemical Reactions in Minerals and Rocks," Dokl. Akad. Nauk **319** (6), 1428–1429 (1991).

32. B. M. Mitsyuk and L. I. Gorogotskaya, *Physicochemical Transformations of Silica Under Metamorphism* (Naukova Dumka, Kiev, 1980) [in Russian].

33. L. V. Sazonova, E. A. Kozlov, and Yu. N. Zhugin, "Distinctive Features of Chemical, Structural, and Phase Transitions in a Plagioclase–Garnet–Pyroxene Rock in Spherical Stress Waves," Geokhimiya, No. 7, 687–694 (1998) [Geochem. Int. **36** (7), 611 (1998)].

34. L. V. Sazonova, E. A. Kozlov, and Yu. N. Zhugin, "Transformation of Quartz–Plagioclase–Garnet–Clinopyroxene Rock in Spherical Stress Waves," in *Proceedings of 26th Lunar and Planetary Science Conference, Houston, USA, 1996* (Lunar. Planet. Inst., Houston, 1996), Vol. 2, pp. 1225–1226.

35. L. V. Sazonova, V. I. Fel'dman, S. P. Fedosova, and N. N. Kononkova, "Some Features of the Garnet Transformations under Shock Metamorphism," Meteoritika, No. 47, 189–196 (1988).

36. L. V. Sazonova, V. I. Fel'dman, E. A. Kozlov, et al., "Genesis of Ringwoodite during Metamorphism Induced by Impact Waves: Experimental Data," Geokhimiya, No. 2, 1–6 (2006) [Geochem. Int. **44** (2), 137 (2006)].

37. L. V. Sazonova, V. I. Feldman, and A. A. Nosova, "Diaplectic Quartz from Autogenous Breccia of the Puchez–Katun Astrobleme (USSR)," in *Proceedings of 13th Lunar and Planetary Science Conference, Houston, USA, 1982* (Lunar. Planet. Inst., Houston, 1982), pp. 681–682.

38. C. H. Simonds, P. J. Floran, P. E. McGee, et al., "Petrogenesis of Melt Rocks, Manicougan Impact Crater, Quebec," J. Geophys. Res. **83** (6), 2773–2788 (1978).

39. D. Stöffler, "Deformation and Transformation of Rock-Forming Minerals by Natural and Experimental Shock Processes: II. Physical Properties of Shocked Minerals," Fortsch. Mineral. **51** (2), 256–289 (1974).

40. G. S. Telegin, V. G. Antoshev, V. A. Bugaeva, et al., "Calculated Determination of Shock Adiabatic Curves for Rocks and Minerals," Izv. Akad. Nauk SSSR, Ser. Fiz. Zemli, No. 5, 22–31 (1980).

41. *Ultrahigh-Pressure Mineralogy*, Ed. by R. J. Hemley, Rev. Mineral. **37** (1998).

42. A. A. Val'ter, G. K. Eremenko, V. N. Kvasnitsa, and Yu. A. Polkanov, *Shock–Metamorphic Carbon Minerals* (Naukova Dumka, Kiev, 1992) [in Russian].

43. S. A. Vishnevskii, V. P. Afanas'ev, K. P. Argunov, and N. A. Pal'chik, *Impact Diamonds: Characteristics, Origin, and Significance* (OIGGiM SO RAN, Novosibirsk, 1997) [in Russian].

44. E. I. Zababakhin, *Problems of Explosive Gasodynamics* (RFYaTs-VNIITF, Snezhinsk, 1997) [in Russian].